HIGH FREQUENCY VARIABILITY IN GLACIER MELTWATER PATTERNS IN THE RHONE WATERSHED, SWITZERLAND

by

Michelle Kristine Meadows

A thesis submitted to the faculty of
The University of Utah
in partial fulfillment of the requirements for the degree of

Master of Science

Department of Geography

The University of Utah

May 2017

The University of Utah Graduate School

STATEMENT OF THESIS APPROVAL

The thesis of **Michelle Kristine Meadows**

has been approved by the following supervisory committee members:

Summer Rupper	, Chair	**2/13/17**
		Date Approved
Richard Forster	, Member	**2/13/17**
		Date Approved
Gregory Carling	, Member	**2/13/17**
		Date Approved

and by **Andrea Brunelle**, Chair/Dean of the Department/College/School of **Geography**

and by David B. Kieda, Dean of The Graduate School.

ABSTRACT

Glaciers contribute to the hydrology of many mountainous watersheds worldwide. Significant attention has been given to seasonal discharge measurements and modeling and relatively little to shorter timescale glacier discharge; thus, our understanding of high frequency variability is more limited. This high frequency variability impacts sediment flux, hydropower generation, montane ecosystems, and so forth. Here we seek to improve our understanding of glacial meltwater processes that control diurnal melt cycles. In particular, we used isotopic and electrical conductivity measurements and discharge estimates in three glaciated watersheds (Rhonegletscher, Gornergletscher, and Langgletscher) and two nonglaciated watersheds within the Upper Rhone Watershed, Switzerland, to test our understanding of diurnal fluctuations and to validate a glacier melt model. We chose these particular watersheds because they represent a significant range in size, shape, slope, and other topographical features that likely impact the shape, magnitude, timing, and duration of daily peak glacial melt. Physical data show differences in magnitude and timing of peak melt between these watersheds. We use a modeling approach to assess the underlying causes of these differences. In particular, we use a temperature index model to calculate hourly melt on each glacier and model meltwater flow on the glacier's surface. The modeled melt volumes were used as input for a watershed model that routed all meltwater to the glacier terminus and the proglacial stream system as surface

flow. The total volume of meltwater reaching the proglacial stream was tracked, and a modeled hydrograph was produced for each glacierized watershed. We used the resulting hydrograph to evaluate which processes are the dominant controlling factors of diurnal melt, focusing on snowpack and exposed ice, to increase our understanding of high frequency melt variability. Results suggested that by the end of the melt season, the shape of the hydrograph was dominantly controlled by air temperature, and ice melt was the primary contributor to total melt volume. The timing of peak melt is strongly influenced by snowpack distribution; when less than 50% of the glacier surface was snow-covered, we observed no delay in the timing of meltwater delivery to the glacier terminus and the proglacial stream system, while the reverse is true as snow cover exceeds 50%. By identifying these parameters at a high temporal resolution, we create a framework to better understand the impact diurnal variations have on various hydrologic, ecologic, and human systems that rely on glacial melt.

TABLE OF CONTENTS

LIST OF FIGURES

Figures

ACKNOWLEDGEMENTS

It would be remiss of me if I failed to acknowledge the many wonderful people who have guided and supported me; I have learned that science really is a group effort. First and foremost, I want to thank my adviser, Summer, for taking a chance on me five years ago as an undergraduate and introducing me to the exciting world of glaciology. Thank you for your countless hours of support and for not giving up on me. A special thanks to my committee, as well. Thank you, Greg and Rick, for always being available to meet and answer questions.

A big thank you to my fellow graduate students, as well. Durban, thank you for sharing your MATLAB expertise and for your help in building my watershed model. It constantly amazes me how efficiently you were able to translate my ideas into code. Additionally, alongside Durban, thank you Eric, Matt, and Kate for assisting me in the field, for always being willing to wade through near freezing water, and for staying up at odd hours of the night to collect water samples.

Last, much gratitude to my wonderful friends and family who always pushed me and supported me through this process. Most recently, thank you for encouraging me through the long hours and late nights, for editing countless thesis drafts, and for your general love and support. Thanks Mom and Dad for supporting me through twenty years of school and for instilling in me the value of an education.

Clearly, I would not have made it without all the amazing people in my life.

INTRODUCTION

Glaciers provide major contributions to water resources in many locations worldwide; many societies and economies rely on river systems fed by glacier meltwater. Glaciers can play a major role in influencing river flux variability. Low frequency climate change controls the variability glaciers impose on hydrologic systems over long timescales. However, glaciers impose variability on many different timescales. While coarser temporal resolutions, such as seasonal, have been well studied the last decade, high frequency variability, such as diurnal, has received less attention.

Diurnal variations in melt dominated stream channels have long been noted; these cycles are now considered a defining characteristic of glacier discharge (Howell, 1953; Meier and Tangborn, 1961; Wendler et al., 1972; Elliston, 1973; Hock et al., 2005). Howell (1953) established a correlation between the amount of solar radiation and magnitude of melt on a glacier surface. Wendler et al. (1972) and Elliston (1973) built on that foundation and observed that peak melt occurred roughly an hour after peak solar radiation and near the time of maximum air temperature measurements for the daily cycle, and peak melt occurred earlier in the day throughout the melt season. Along with timing of peak melt, fluctuations in hydrochemistry of meltwater have been well studied, and it is now well understood that peak discharge in proglacial streams is characterized by a depleted isotopic signature, low electrical conductivity, and low solute concentrations (Collins, 1979; Brown, 2002). The onset of glacial modeling

allowed further study of these fluctuations. A majority of these models (physical and empirical) run on daily, monthly, and, for longer term studies, yearly timescales. Few employ shorter (hourly) time resolutions. Many of these studies have analyzed the effects of diurnal discharge on proglacial stream systems, quantified glacier meltwater contributions to these stream systems, and focused on the implications models have on subglacial drainage systems (e.g., Arnold et al., 1998; Flowers and Clarke, 2002; Singh et al., 2005; Mark and Seltzer, 2003). Few have studied the physical processes that control the shape and timing of these cycles. Willis et al. (2002) concluded that the snowline elevation affected the shape of the proglacial hydrograph; yet the same shape is observed when snow melt is removed from the total melt volume. The dearth of research on diurnal cycles raises the question: What physical processes control the shape and timing of these cycles? Here we seek to identify the processes driving diurnal variations using a suite of observations in three glacierized watersheds of different shape and size in combination with two models, a glacier melt model and a watershed model. Constraining our understanding of these fluctuations may influence melt forecasts and watershed management, which could have profound effects on the power sector, agriculture, and communities that rely on meltwater for drinking water and other purposes.

One glaciated watershed of societal importance is the Rhone Watershed, covering southwest Switzerland and southeast France (see Figure 1). Originating in the Swiss Alps, the Rhone River forms from dozens of glacier-derived tributaries, flows into Lake Geneva, continues southwestward into France, and eventually discharges into the Mediterranean Sea. Within the Rhone Watershed, agriculture, industry, energy, tourism, and transportation rely on the river system.

Headwaters of the Rhone River are within the heavily glacierized Upper Rhone Watershed (see Figure 2). Current estimates suggest these glaciers make significant contributions to Rhone River flux (Klok et al., 2001). Some individual glacier contributions have been studied in detail, such as contributions from the Rhonegletscher. In particular, Klok et al. (2001) estimated that 61% of the Rhone River's total annual discharge, measured at a point 2.5 km downstream of the Rhonegletscher, was glacially derived. Earlier studies (Elliston, 1973) estimated that glaciers contributing to the Matter-Vispa, a tributary to the Rhone River, accounted for 35-60% of total discharge. This suggests that, at least for portions of the Rhone River, glacier contributions to the river flux can be significant.

If glacier contributions are indeed significant, climate change will inevitably affect the Rhone Watershed through glacier change. On average, Swiss temperatures rose 0.11°C/decade since the late 1800s (Ceppi et al., 2009). However, mountainous regions experienced more drastic changes than other areas, with some locations reporting a 2°C temperature change over the last century. By 2100, this could increase to a 4°C winter temperature change and a 6°C summer temperature change (Beniston et al., 2011). As a result, melt rates will increase and peak seasonal melt will occur earlier in the melt season, altering water flux patterns in rivers down-valley (Pellicciotti et al., 2010; Finger et al., 2012; La Frenierre and Mark, 2014). Additionally, as glaciers continue to shrink, each catchment will reach a critical threshold in which meltwater contributions will begin to decline. Several glacierized catchments have already experienced this decline (Stahl and Moore, 2006; La Frenierre and Mark, 2014). While we understand the potential affects this phenomenon could have on seasonal and annual discharge, we have little

knowledge as to the effect this could have on diurnal fluctuations. By understanding drivers in the system and physical processes that control these higher frequency variations, we may better forecast future diurnal discharge scenarios and the effect on hydropower, agriculture, and downstream communities whose livelihoods rely on glacier meltwater.

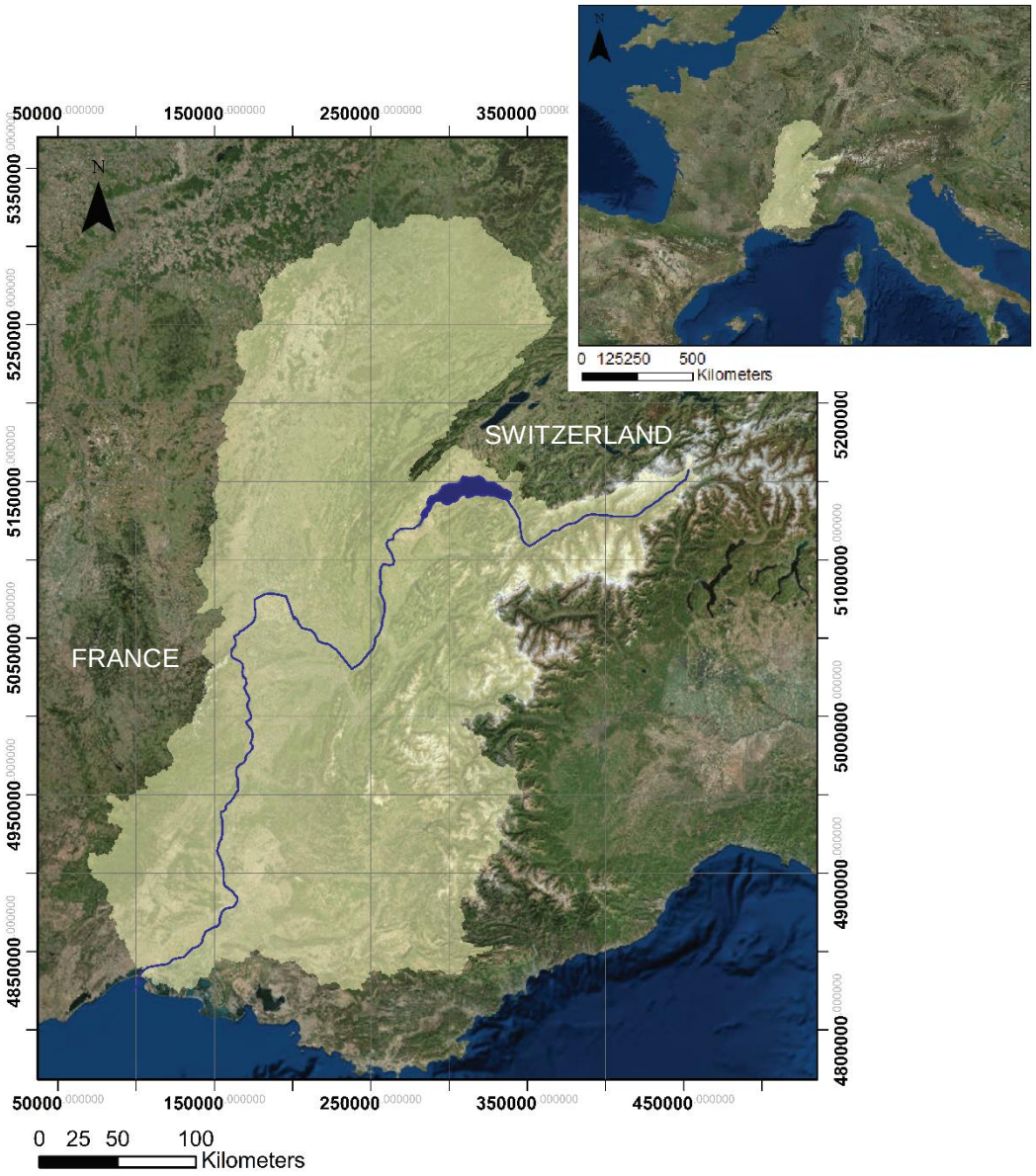

Figure 1. The Rhone Watershed. The watershed area is shaded in yellow, with the glacierized area shaded in blue (GLIMS, 2015).

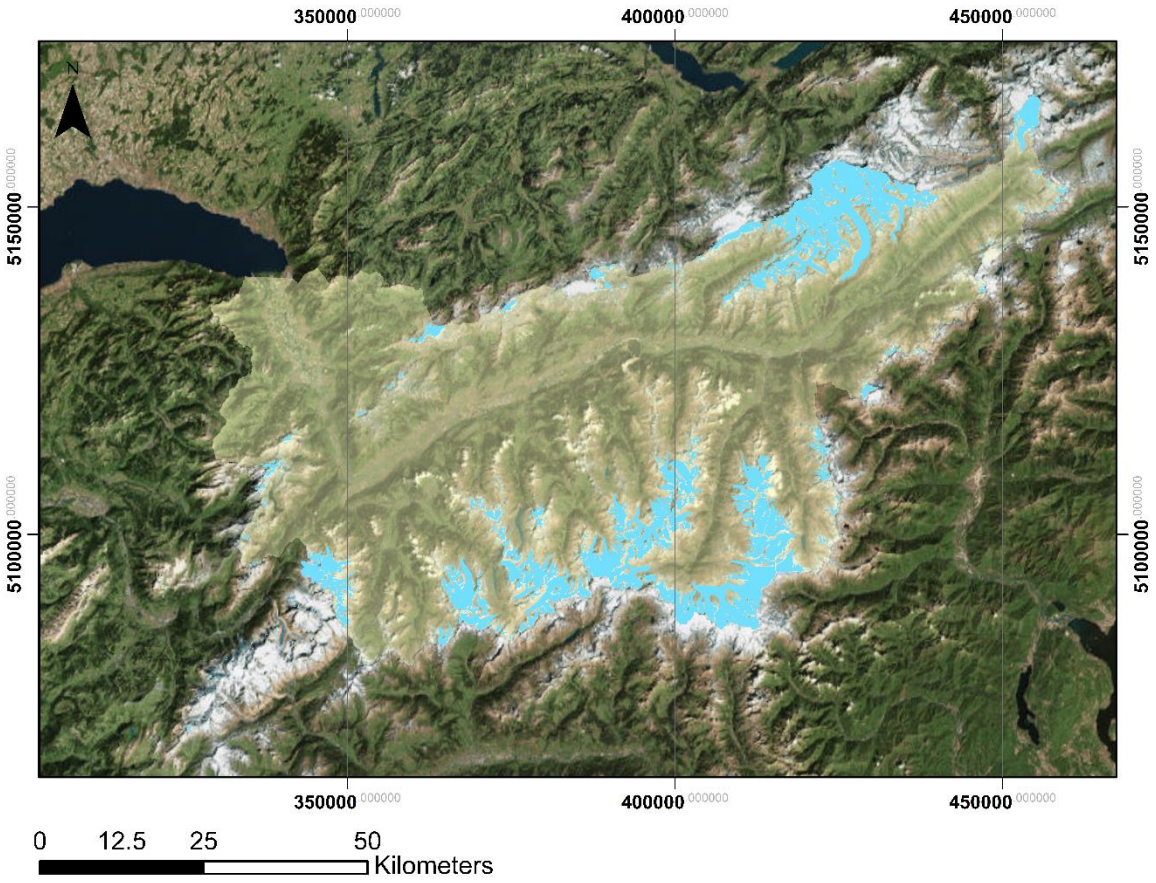

Figure 2. The Upper Rhone Watershed. The watershed area is shaded in yellow, with its contributing glaciers shaded in blue (GLIMS, 2015).

STUDY AREA

We chose three glacierized and two nonglacierized catchments within the Upper Rhone Watershed. The three glacierized catchments (Rhonegletscher, Langgletscher, and Gornergletscher) represent various glacier sizes, shapes, and slopes that may affect the timing of meltwater delivery to the glacier terminus. The two nonglacierized catchments (sampled near Ulrichen and Binn, Valais, Switzerland) act as necessary controls used to determine the magnitude of variation due to the presence of glaciers in a catchment and provide information on variability present in the absence of glaciers.

Glacierized Watersheds

As the source of the Rhone River, the Rhonegletscher remains a vital component of the hydrologic system within the Upper Basin (see Figure 3). The Rhonegletscher is one of the most studied glaciers in the region, with continuous mass balance calculations since 1874 and recorded length variations since the 17th century (Mercanton, 1916; Bonney, 1917; Stroeven et al., 1989). After reaching its maximum neoglacial length during the Little Ice Age in 1602, the Rhonegletscher has retreated nearly continuously through the 21st century, with the exception of intermediate advances between 1800 and 1856 (Mercanton, 1916; Bonney, 1917; Roethlisberger, 1963; Stroeven et al., 1989; Glaciological Reports, 2015). Between 1878 and 2000, the Rhonegletscher retreated 1700 m and decreased in thickness by approximately 50 m, and models suggest a negative

mass balance trend since the 1860s (Sugiyama et al., 2007; Huss et al., 2008).

The Langgletscher, located 40 km to the west of the Rhonegletscher in the Lötschental Valley, forms from two source glaciers: the Anungletscher and a second, smaller, unnamed tributary (see Figure 4). Both are considered components of the Langgletscher as they converge and flow in the lower half of the glacier system. The Langgletscher is the source of the Lonza River, a tributary to the Rhone River. Though not as heavily researched as the Rhonegletscher, studies report a 10.1% surface area loss between 1977 and 2005 with the glacier tongue steadily retreating (Collins, 2006; Glaciological Reports, 2015).

As the second largest glacier system in the Alps after the Aletsch system to the north and main source of the Matter Vispa, a large tributary to the Rhone River, the Gornergletscher is fed by several tributary glaciers (Monte Rosa Gletscher, Grenzgletscher, Zwillingsgletscher, Breithorngletscher, Triftjigletscher, and Unterer Theodulgletscher); however, the Gornergletscher is now disconnected from its tributaries, and the Grenzgletscher dominates the system (see Figure 5). According to the Swiss Glacier Monitoring Network, the Gornergletscher has retreated approximately 3000 m since 1882 (Swiss Glacier Monitoring Network, 2015).

Ultimately, these three glaciers were chosen to represent variations in shape, size, slope, and aspect of glaciers. The hypsometry (area-to-altitude relationship) of each glacier is shown in Figure 6. Table 1 outlines physical characteristics of the glaciers. The Gornergletscher is the largest glacier system and also has the highest percent glacierized watershed. The Langgletscher is the smallest system with the smallest percent glacierized watershed. It is also the steepest glacier, and the Rhonegletscher has the most gradual

incline. These differences contribute to the robustness of the model and allow us to make more conclusive statements regarding physical processes that control diurnal variations.

Nonglacierized Watersheds

In addition to glacierized catchments, we studied two nonglacierized (or minimally glaciated) catchments as controls. These control groups were used to analyze base flow and compare glacial diurnal variations to other variations within the system, such as seasonal snowmelt, evapotranspiration, storm peaks, etc.

One nonglacierized (or minimally glaciated) watershed chosen was the area surrounding the Binna River, an 18 km long tributary to the Rhone River. The entire watershed, shaded in yellow in Figure 7, covers 43.68 km^2 from the sample location and upwards, and 2.1% of the watershed is glaciated.

The second nonglacierized catchment studied was the area contributing to the main stream system in the Oberbach Valley, a small valley entering the Rhone River from the north in the village of Ulrichen (Figure 8). The catchment area is devoid of glaciated areas and thus is derived completely from sources other than glacier melt. As the smallest watershed, it covers an area of 3.53 km^2.

These two watersheds were chosen for locational and physical purposes. Many accessible valleys with stream systems large enough to study are glaciated; thus, options were limited. However, these two nonglacierized watersheds were both accessible with high flow rates. Additionally, they represent watersheds of different sizes, slopes, and aspects and represent nonglacierized valleys in both the northern (Ulrichen) and southern (Binna River) zones of the Upper Rhone Watershed.

Figure 3. Aerial View of the Rhonegletscher. The glacierized surface, shaded in blue, and the surrounding watershed, shaded in yellow, are outlined. The orange dot represents the lowest elevation of the watershed.

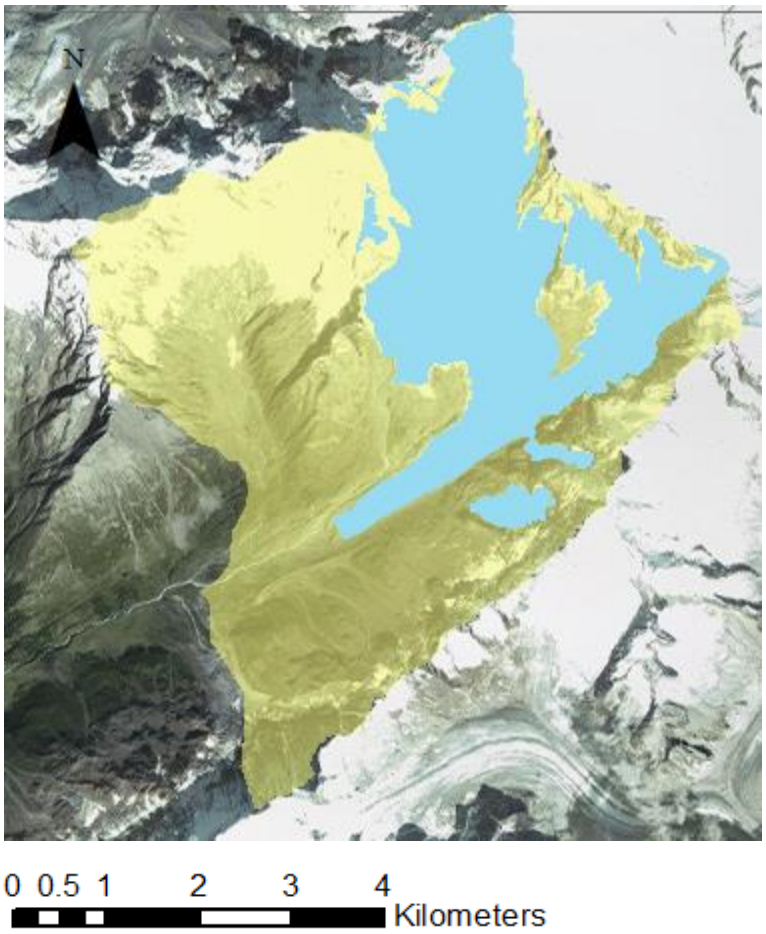

Figure 4. Aerial View of the Langgletscher. The glacierized surface is shaded in blue, and the surrounding watershed shaded in yellow. The orange dot represents the lowest elevation of the watershed.

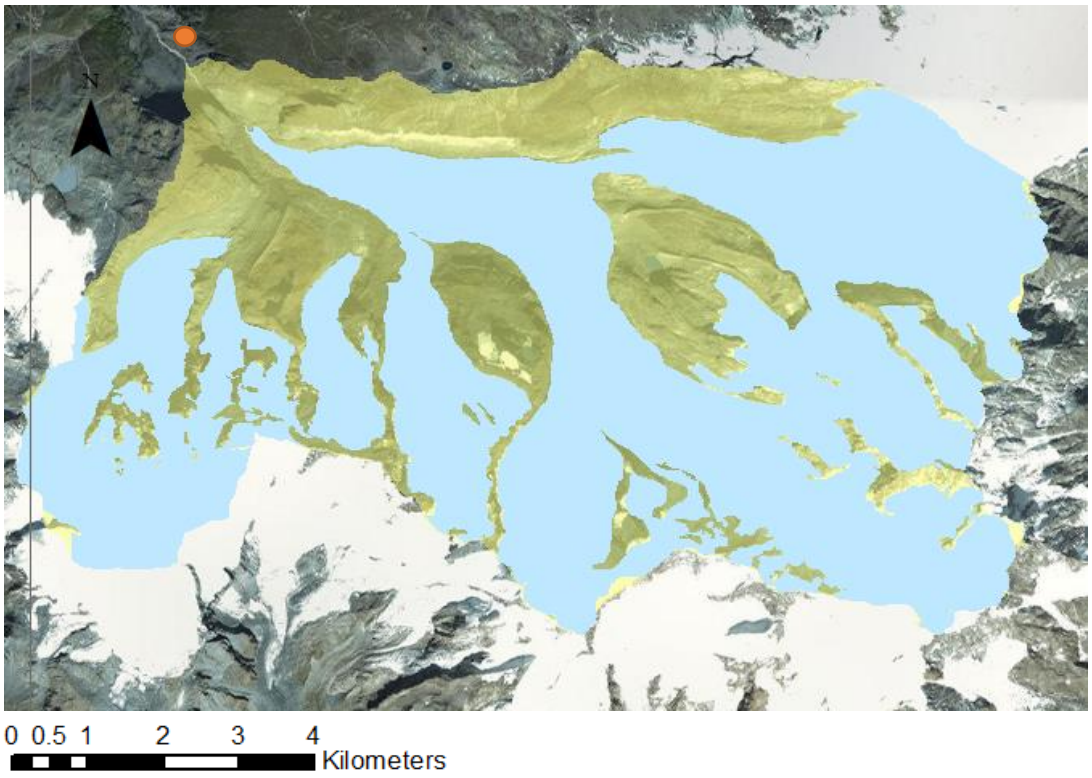

Figure 5. Aerial View of the Gornergletscher. The glacierized area is shaded in blue and the surrounding watershed shaded in yellow. The orange dot represents the lowest elevation of the watershed.

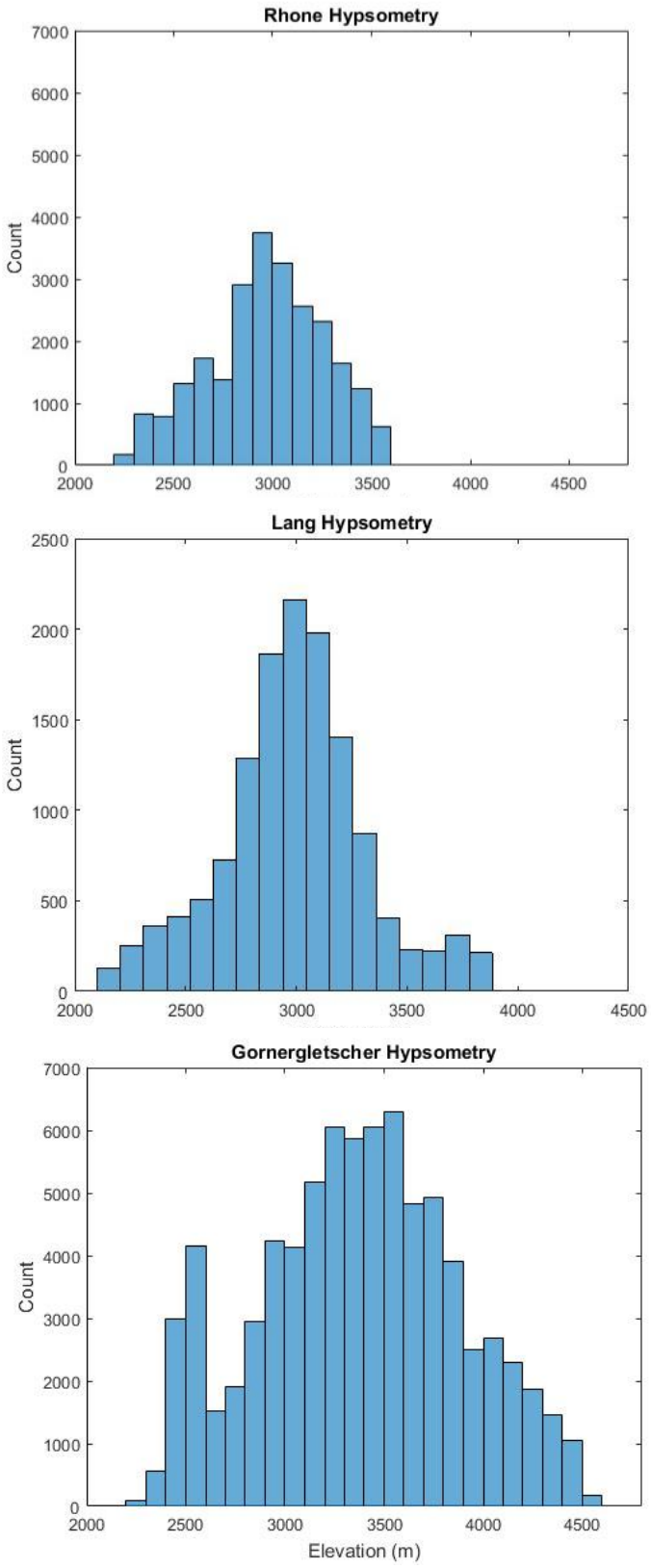

Figure 6. Glacier Hypsometries. These figures illustrate the area to altitude relationship of each glacier.

Table 1. Physical characteristics of each glacier. The distance between the toe and the lowest elevation is the distance between the glacier terminus and the lowest elevation of the watershed.

	Rhone	Lang	Gorner
Maximum Elevation	3599 m	3874 m	4561 m
Minimum Elevation	2229 m	2125 m	2235 m
Mean Elevation	2995	2947 m	3337 m
Snowline Elevation	3060	3022 m	3573 m
Mean Slope	19.3°	23.5°	22°
Mean Aspect	183.3°	194.6°	219.6°
Length	8.5 km	6 km	12 km
Glacier Area	16 km^2	10.9 km^2	51.59 km^2
Watershed Area	26.58 km^2	29.98 km^2	78.85 km^2
Percent Glacierized	60%	38%	65%
Distance between Toe and Lowest Elevation	0.98 km	1.58 km	1.45 km
Distance to Weather Station (WS)	3 km	7.5 km	0 km
Elevation Change between Glacier Toe and WS	-300 m	-600 m	+600 m

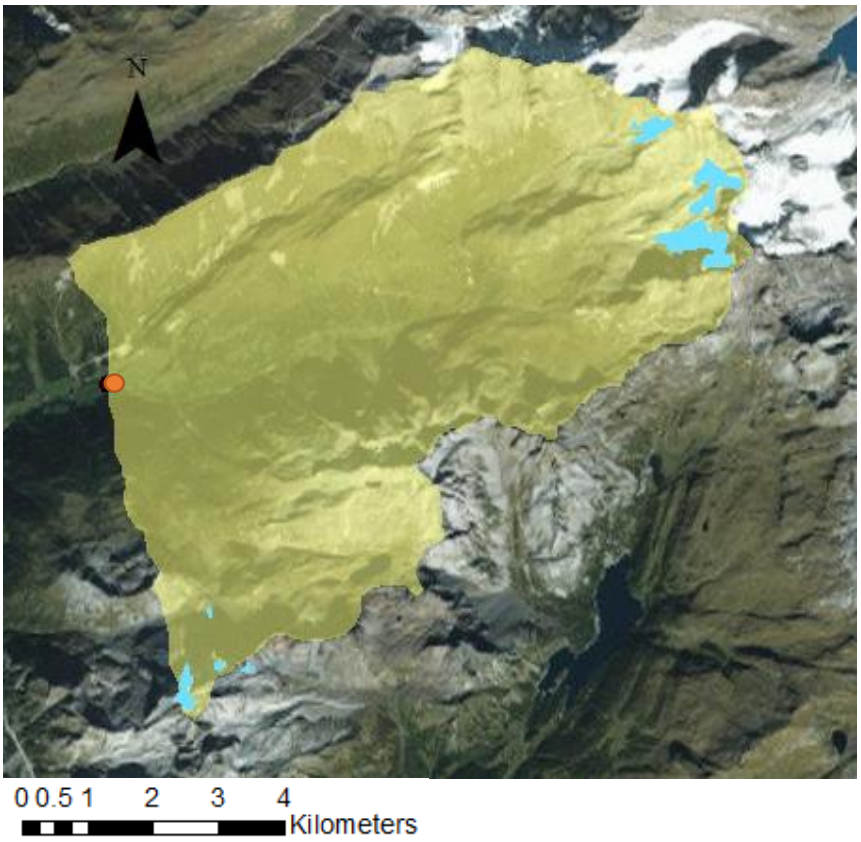

Figure 7. Aerial View of the Binna River. The orange dot represents the lowest elevation of the watershed.

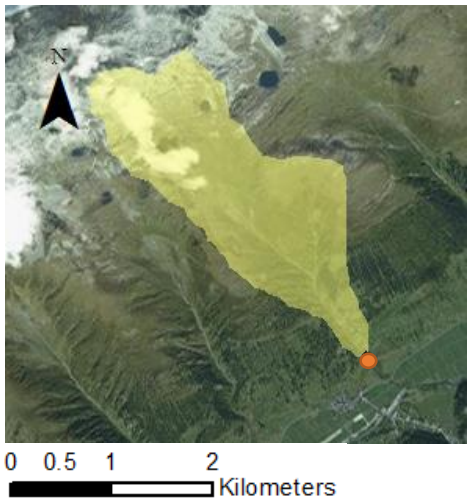

Figure 8. Aerial View of Ulrichen. The orange dot represents the lowest elevation of the watershed.

METHODOLOGY

At each of the five watersheds described above, we installed pressure transducers at the bottom of the stream beds, measured electrical conductivity of stream water, and sampled stream water for isotopic analysis. The pressure transducers recorded changes in water height over the course of 19 to 20 days. This data was then used as an analog to streamflow and discharge measurements, essentially providing the shape of the hydrograph for each watershed. The total dissolved solids concentration, measured through electrical conductivity, along with isotopic measurements, were used as indicators of water source. We used temperature data and surface measurements such as slope and aspect to help inform a numerical model that calculated meltwater volumes over the surface of the glacierized area in each watershed. The model then routed meltwater down the surface of the glacier and into the stream system. We tracked the total volume of modeled meltwater entering the stream system each hour, and with that output created modeled hydrographs for each glacierized catchment. We compared the modeled hydrograph to the transducer data to test the robustness of the model and determine if the model captured the same peak timing and overall shape as the measured data.

Field Work

All fieldwork was completed in August 2015. Late summer was chosen in order to capture maximum late summer ice melt and minimum snow melt contributions. By late summer, snowlines are at their maximum elevation, and melt is presumably predominately glacier ice. All installations and water sample collections were completed within 2 km of the glacier terminus to minimize the influence of nonglacial water sources. Pressure transducers were installed at the base of the stream beds. The transducers recorded pressure and water temperature every five minutes for approximately 20 days in August 2015. When stream levels rise, the pressure increases; thus, pressure data is used as an analog to stream discharge. Atmospheric pressure was accounted for using a combination of daily weather station data, 6-hour ERA Interim data, and altitude corrections using Equation 1 (Portland State Aerospace Society, 2004):

$$P = P_0 \left(1 - \frac{Lh}{T_0}\right)^{\frac{gM}{R_0 L}} \quad (1)$$

where L is the standard temperature lapse rate for dry air, h is the elevation of the sample location, T_0 is standard temperature at sea level, M is the molar mass of dry air, and R_0 is the universal gas constant.

To determine if the majority of the stream water measured was glacially derived, electrical conductivity measurements and water sampling for isotopic analysis were required. Water samples were collected for stable water isotope analysis at the same site as the pressure transducer locations. These samples were collected every hour for a 24-hour period at each sample location. In addition, electrical conductivity and air

temperature were recorded at the same interval as the water sampling. Stable water isotopes and electrical conductivity measurements were used together to determine what fraction of the stream water was glacially derived. Glacier meltwater has a low total dissolved solids concentration and thus a low electrical conductivity measurement. The conductivity of glacier meltwater is typically on the order of 10^1 µS cm^{-1} while the conductivity of subglacial water is higher and can reach 10^2 µS cm^{-1}; thus, electrical conductivity is an excellent indicator of water source (Collins, 1979). The isotopic signature of glacier meltwater is complex due to varying fractions of snow melt and ice melt, evaporation and sublimation on the surface, melting, and recrystallization (Ofterdinger, 2001). Therefore, we instead analyzed relative temporal variations in isotopic signatures rather than the isotopic values at each hour. Any significant fluctuations or diurnal signals observed may indicate a change in water source. Determining the source of the water at the measurement sites is important. If these data provide evidence that the water is glacially derived, then we can interpret the pressure transducer data in terms of glacier melt entering the stream system and focus modeling on physical processes that control meltwater delivery.

Laboratory Analysis

Water samples were brought back for stable water isotope analysis (specifically $\delta^{18}O$) to help determine water sources throughout the day. Water samples were analyzed at Brigham Young University using a Los Gatos Cavity-Ringdown and corrected for instrumental drift using international standards. Uncertainties for the particular instrument are +/- 0.20‰ for $\delta^{18}O$ and +/- 1.0‰ for δD.

Data Acquisition

While the observational data provides important insights into the high frequency variations of glacierized and nonglacierized streams and information on water source, physical models are critical to evaluating the underlying physical processes driving the variations. Here we describe the data required to drive the model. In particular, the model required DEMs, snowlines for each watershed as boundary conditions, and hourly temperature data to drive the melt model.

DEMs

We acquired 2011 ASTER Global Digital Elevation Maps (DEMs) with a 30 m spatial resolution for each watershed (NASA/METI, 2011). DEMs for the entire Upper Rhone Watershed were compiled, and data for individual watersheds were clipped from watershed and glacier shapefiles (GLIMS, 2015).

Snowlines

Snowlines for each glacier were calculated using Landsat 5 imagery from August 2015 (NASA LP DAAC, 2011). We used images containing less than 10% cloud cover that were captured over the course of the sampling period, and then calculated average snowlines during the month of August. This was done by first building composite rasters of Bands 1, 4, and 5 (blue, near infrared, and shortwave infrared, respectively) from low cloud cover Landsat imagery. We then used a supervised maximum likelihood classification to distinguish between snow and ice in the images. After the classifications were completed, a snowline was defined as the boundary between snow and ice polygon

classes, and the elevation of the snowline was extracted at 50 m intervals using ASTER DEMs, as dictated by Keeler et al. (2015).

Temperatures

Hourly temperature data, one of the key model inputs, was acquired from MeteoSwiss weather stations near each glacier. Data from the Grimsel Hospiz station was used for the Rhonegletscher. This weather station is located at 1980 m a.s.l., approximately 300 m below the elevation of the glacier terminus and approximately 3 km from the glacier on a ridge above the valley. For the Langgletscher, data from the Blatten station was used, located at 1538 m a.s.l., approximately 600 m beneath the elevation of the glacier terminus and 7.5 km down-valley from the glacier. Last, for the Gornergletscher, data from the Monte-Rosa-Plattje station was used. The station is located at 2885 m a.s.l., situated approximately 600 m above the glacier terminus on exposed rock between the Gornergletscher and the Grenzgletscher, a tributary to the Gorner. The satellite data and meteorological data provided all necessary inputs for the melt and watershed model.

Temperature Index Model

Alongside the physical data, a melt model, watershed model, and hydrograph generation were used to understand drivers in the system and identify any differences between the three glacierized watersheds. Using this combination of models, we have the ability to run sensitivity tests on each glacier and isolate factors that may potentially affect the timing of meltwater delivery to the stream system below. First, to calculate the

melt volumes across the surface of each glacier each hour, we applied an hourly temperature index model adapted from Hock (1999). Rather than dividing a degree-day factor by the number of time steps per day, we used hourly melt factors calculated by Gabbi et al. (2014). This temperature index model included potential clear sky solar radiation. Stroeven et al. (1989) suggest glaciers in the Alps follow the mean Northern Hemispheric temperature trend, intimating that the glaciers react to solar radiation variations more readily than to local temperature and precipitation variations. By employing a temperature index model that includes solar radiation, results closely approximate that of an energy balance model, yet the temperature index model does not have the same intensive data requirements as a full energy balance model. Thus, we justified its use.

Here we solved for meltwater per hour in mm (M) at each DEM cell across the glacier surface:

$$M = \begin{cases} \left(MF + \propto_{snow,ice} I\right) T, & T > 0 \\ 0, & T \leq 0 \end{cases} \quad (2)$$

where MF is the hourly melt factor (mm h^{-1} °C^{-1}), $\alpha_{snow,\ ice}$ is the radiation factor for a snow- or ice-covered surface, respectively (mm m^2 h^{-1} W^{-1} °C^{-1}), I is the potential clear sky direct solar radiation (Wm^{-2}), and T is air temperature (°C). The temperature at each glacier DEM cell each hour was calculated by extrapolating temperature data from the nearest weather station to each glacier, using a regional temperature lapse rate of -0.56°C per 100 m (Richard and Tonnel,1985). The potential clear sky direction solar radiation is calculated in Equation 3 and is a function of solar geometry, surface topography, and

atmospheric properties (Hock, 1999):

$$I = I_0 \left(\frac{R_m}{R}\right)^2 \varphi_a^{\left(\frac{P}{P_0 cosZ}\right)} cos\theta \quad (3)$$

where I_0 is the solar constant, R_m is the mean earth Earth-Sun distance, R is the instantaneous Earth-Sun distance, and the ratio of the two is the eccentricity correction factor, φ_a is the mean atmospheric clear sky transmissivity, P is the atmospheric pressure and is calculated using Equation 1, P_0 is mean atmospheric pressure at sea level, Z is the local zenith angle, and θ is the angle of incidence at the DEM cell every hour. The Earth-Sun distance is simply a function of time of year. Z and θ are calculated as functions of surface topography and time of day (Iqbal,1983; Hock, 1999). All constants and units are listed in Table 2.

Once temperatures were extrapolated to each DEM cell and solar radiation was calculated for each DEM cell, the temperature index model was used to derive melt volumes each hour for each glacier cell. The resulting output of the melt model was then used as input to a watershed model.

Watershed Model

A watershed model was used to direct meltwater from its DEM cell to the glacier terminus and into the stream system as surface flow; in reality, large volumes of meltwater enter the glacier through moulins and crevasses and flow to the terminus through subglacial conduits. Using a DEM of the watershed, we created a stream system across the watershed that directed the flow of meltwater across the surface. The model

then calculated the time it took meltwater from each cell each hour to reach the stream system. With this information, the model tracked the total volume of meltwater entering the stream system each hour and generated a hydrograph at the sample location.

First, the ASTER DEMs were imported into MATLAB. Using Topotoolbox, an open source MATLAB toolbox (Schwanghart and Scherler, 2014), we derived a stream system covering each DEM cell using slope and aspect to determine the flow direction for meltwater occurring at each cell each hour across the entire watershed. We then calculated flow accumulation values along each cell. For each cell, we used Topotoolbox to calculate the number of upstream cells based on the flow direction output. The larger the number of upstream cells, the larger the flow accumulation value. Once the stream system was created, the flow velocity at each cell was calculated using a model derived by Arnold et al. (1998), briefly described below. The flow velocity in this model depends on surface characteristics (e.g., snow- or ice-covered or moraine material) according to Equations 4-6:

$$D = \frac{\kappa_e d}{\left(\frac{3\rho_w g}{\mu}\right)^{\frac{1}{3}} k^{\frac{1}{3}} q^{\frac{2}{3}}} \tag{4}$$

$$V_s = \left(\frac{\rho_w g}{\mu}\right) k\theta/\kappa \tag{5}$$

$$V_{i/m} = \frac{R^{\frac{2}{3}} \theta^{\frac{1}{2}}}{n_{i/m}} \tag{6}$$

Equation 4 calculates the time it takes meltwater on the surface of snowpack to

percolate down to the base of the snowpack (Colbeck, 1978), where D is the travel time (s), κ_e is the snow effective porosity, d is the snowpack depth, ρ_w is the water density, g is gravity, μ is water viscosity, k is the snow permeability, and q is the flux of meltwater traveling through the snowpack. Values for each constant are given in Table 2 and represent "medium grain old dry snow" (Male and Gray, 1981). Snow depths at each cell above the snowline were assigned a value between 0 and 8 m as a linear function of altitude. A maximum snow depth of 8 m was chosen to reflect a mean snow depth of 2-3 m across the glacier surface during the melt season (Kuhn et al., 1998; Machguth et al., 2006; Helfricht et al., 2013)

Equation 5 calculates the velocity of meltwater on a snow covered cell (Colbeck, 1978), where κ is the snow porosity and θ is the slope of the DEM cell. The meltwater is treated as overland flow, saturating layers of snow right above the ice layer and flowing laterally (Fountain, 1996).

Equation 6 calculates the velocity of meltwater on a bare ice surface (V_i) or moraine surface (V_m) (Colbeck, 1978), where R is the hydraulic radius of the meltwater channel and $n_{i/m}$ is the Manning's roughness coefficient for an ice or moraine surface. In this equation, meltwater is routed through the channel system created within the watershed model. The hydraulic radii of the channels on both ice and moraine surfaces were calculated as a linear function of the flow accumulation values discussed previously. The larger the number of contributing upstream cells, the larger the hydraulic radius. The lowest flow accumulation values, associated with the smallest flow accumulation values, were assigned a hydraulic radius of 0.024, created to represent a stream with a width of 0.24 m and depth of 3 cm. The highest flow accumulation values

were assigned a hydraulic radius of 0.167, representing a stream with a diameter of 2 m and a depth of 20 cm. These values are theoretical rather than empirical and thus lead to some uncertainty. It is possible to over- or underestimate the hydraulic radius and that radius' ability to transport any given volume of meltwater across the glacier surface without delay. However, changes in the hydrograph shape due to variations in the hydraulic radius are negligible until the radius is decreased by two orders of magnitude (see Figure 9). Thus, the results are unlikely to change significantly within the physically realistic range of hydraulic radii used here (Arnold et al., 1998). Roughness coefficients for ice surfaces and a stony river channel were chosen to represent glacial surfaces and moraine surfaces, respectively.

Due to its poor sorting and low porosity and permeability, we assumed surface flow, though we acknowledge that some water can flow through the material. Alternatively, water on the moraine surface can be treated as groundwater flow. For this scenario, we used Equation 7 to calculate the velocity (V) of groundwater through a moraine system:

$$V = tan\theta / K \tag{7}$$

where θ is the slope of the DEM cell and K is the hydraulic conductivity of the moraine material.

Once individual cells were assigned a flow equation depending on their surfaces (snow, ice, or moraine), the meltwater each hour was then routed downstream to the base of the watershed (i.e., the sample location) using the equations above. Once the meltwater

left the glacier and entered the river system, Equation 6 was used with the maximum hydraulic radius calculated in order to determine the velocity of meltwater in the streambed. As shown in Figure 9, increasing the hydraulic radius would have a negligible effect on velocity calculations. We calculated the time it takes for meltwater in each DEM cell to flow across the glacier surface, into the stream system, and to reach the sample location, and with the time calculations and corresponding melt volumes per hour, we created hydrographs for the entire sampling period at the sampling location. The modeled hydrographs were then compared to measured data to evaluate model limitations. In addition, sensitivity tests helped determine factors that might control the hydrograph shape and timing of peak melt, such as snowpack depth, snowpack distribution, moraine flow, air temperature, and slope.

Table 2. Values and constants used in the temperature index model and flow equations.

Constant	Value	Units	Source
MF	0.11	-	Gabbi et al., 2014
α_{snow}	0.0003	mm m^2 h^{-1} W^{-1} $°C^{-1}$	Gabbi et al., 2014
α_{ice}	0.0005	mm m^2 h^{-1} W^{-1} $°C^{-1}$	Gabbi et al., 2014
I_O	1368	W m^{-2}	Frölich, 1993
ψ_a	0.75	-	Hock, 1999
P_O	101325	Pa	-
R_m	1.496e8	Km	-
R	1.513e8	Km	-
κ_e	0.63	-	Arnold et al., 1998
d	0 – 5	M	-
ρ_w	1000	kg m^{-3}	-
g	9.81	m s^{-2}	-
μ	1.8e-3	Pa s	Arnold et al., 1998
k	6e-9	m^2	Arnold et al., 1998
q	Model results	m^3 s^{-1}	-
κ	0.68	-	Arnold et al., 1998
θ	Slope of DEM cell	-	-
R	0.035 – 0.167	M	-
n_i	0.05	$m^{-1/3}$ s	Arnold et al., 1998
n_m	0.035	$m^{-1/3}$ s	-
L	0.0065	K m^{-1}	-
T_0	288.15	K	-
M	0.0289644	Kg mol^{-1}	-
R_0	8.31447	J mol^{-1} K^{-1}	-
K	0.1	M s^{-1}	-

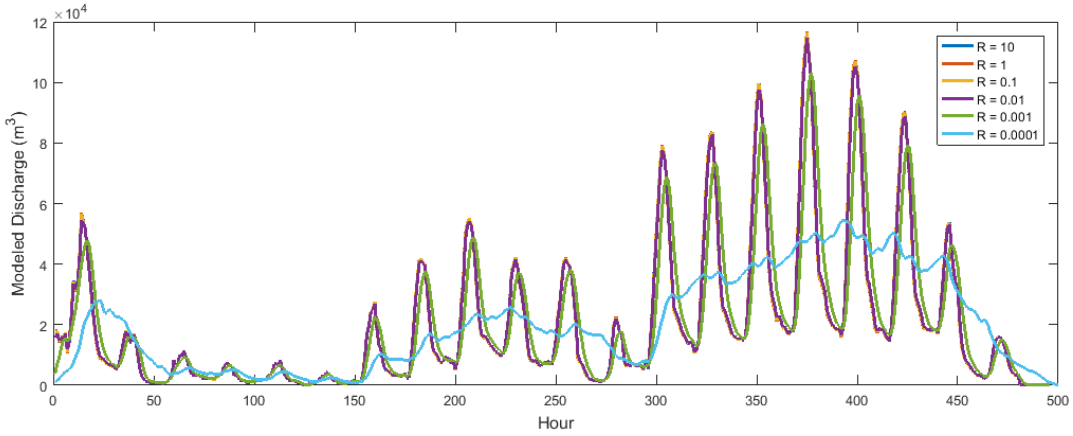

Figure 9. Hydrographs with Varying Hydraulic Radii. As hydraulic radius increases, the smaller the variation observed. In this model, variation only occurs when hydraulic radius is decreased by two orders of magnitude.

RESULTS

Field Measurements

Pressure Data

As part of this study, we measured water level, electrical conductivity, and collected water samples for laboratory analysis in the field. Figure 10 shows recorded water level data from two glacierized streams beneath the Rhonegletscher and Langgletscher and from the two nonglacierized watersheds, the Binna River and Ulrichen. We were unable to acquire pressure data from the Gornergletscher due to time restraints. We identify strong diurnal fluctuations near the terminus of the Rhonegletscher and Langgletscher, characteristic of glacier-fed stream systems (Hock et al., 2005). The timing of peak pressure for both the Rhonegletscher and Langgletscher is nearly synchronous despite the differences in glacier size, slope, and hypsometry. Although the Langgletscher tends to reach peak pressure 1-2 hours before the Rhonegletscher, some diurnal cycles show no offset between the two. The range of variation recorded in the Langgletscher data are much larger than the Rhonegletscher as well, though this may result from differences in river morphology rather than differences in stream discharge and thus should not be interpreted as differences in magnitude of runoff. Each has an asymmetrical shape with rapid onset to peak pressure, followed by a slow decline in pressure throughout the day.

We interpret sharp increases found in the nonglacierized watersheds' data as storm events. This interpretation is corroborated by local weather station data. We note diurnal fluctuations at the two nonglacierized sites, though of significantly smaller magnitudes and with smaller, broader peaks. Moreover, peak pressure in the nonglacierized sites is offset from the glacierized catchments. The dampened and offset diurnal signal observed in nonglacierized streams is likely due, in part, to evapotranspiration (Bren, 1997; Gribovszki et al., 2010). The difference in magnitude of diurnal fluctuations observed in the physical data between the two glacierized and the two nonglacierized watersheds reveals the role glaciers play in these variations. To further investigate this observation, we analyzed the electrical conductivity measurements and isotopic signatures to ensure that a majority of water flowing through the glacierized watersheds' stream systems is glacially derived.

Electrical Conductivity

The 24-hour electrical conductivity data from the glacierized watersheds (Langgletscher and Gornergletscher) are shown in Figure 11, and the measurements from the two nonglacierized watersheds are shown in Figure 12. We lack electrical conductivity from the Rhonegletscher due to instrumental error. The diurnal signal is strongly present in the two glacierized watersheds, with the highest electrical conductivity in the morning hours when glacial melt is at a minimum. We observe no significant diurnal cycle in the nonglacierized watersheds' electrical conductivity data; what variability does occur is of much smaller magnitude than that of the glacierized watersheds.

Electrical conductivity measurements from the Langgletscher are significantly higher than the Gornergletscher though still within reason for a glacierized watershed (Collins, 1979). These differences are attributed to differences in local geology. The Langgletscher, located in the northern half of the Upper Rhone Valley, lies within the Helvetic Zone of the Alps. This zone is composed of marine limestone, marl, and shale. The Gornergletscher, however, is located in the southern half of the Upper Rhone Valley, which lies within the Penninic Zone of the Alps. This zone is composed of high grade metamorphic rocks; ophiolite sequences and schists dominate this region. We would expect higher electrical conductivity measurements in waters interacting with carbonate rocks compared to metamorphic rocks.

Glacier meltwater contributions that have not interacted with the bed of the glacier have much lower total dissolved solids concentrations and thus lower specific conductance. The data indicate that glacial meltwater dominates the system during the daytime hours when electrical conductivity is at a minimum, while another system, possibly a groundwater system or subglacial contributions with higher ionic concentrations, dominates during the night. In addition to electrical conductivity measurements, isotopic data is then used to further analyze water sources throughout the day.

Isotopes

We measured stable water isotopes in each water sample to help determine the source of the stream water. Figure 13 shows all isotope measurements from the three glacierized and two nonglacierized watersheds. All measurements plot near the global

meteoric water line (GMWL, see Equation 8), suggesting that the bulk of the water is derived from precipitation sources and has undergone minimal evaporation and geothermal exchange (Craig, 1961):

$$\delta D = 8\, x\, \delta^{18}O + 10 \quad (8)$$

The isotope measurements are separated out by watershed in Figures 14 and 15. The isotopic signatures vary in each watershed, with no clear diurnal cycle. We observe depleted values in both glacierized and nonglacierized watersheds, consistent with the signatures of glacier ice and local rainwater (see Table 3), as a result of temperature and altitude. As stated previously, the isotopic signature of glacier meltwater is complex owing to spatial variations in measurements across the surface, varying contributions of snow and ice melt, and thermodynamic processes (see variation in isotopic signatures in glacier ice in Table 3). The data suggests, due to lack of diurnal variation, a constant water source. The electrical conductivity data suggests multiple sources; however, while not surface melt, the overnight source is glacially derived. This source may be a shallow groundwater system or subglacial contribution to the stream system that both ultimately originated from glacial melt. Given the high likelihood that the majority of the river flux is glacially derived for the three glacierized watersheds, we use the melt and watershed models to assess the physical processes driving the proglacial hydrograph shape and timing.

Modeled Results

We applied the melt and watershed model to the three glaciated watersheds. Using the models and resulting hydrographs, we created scenarios that best capture the timing of peak melt and the proglacial hydrograph shape exhibited in the pressure transducer data for each watershed. Results help identify drivers of the diurnal cycle within the system and further our understanding of the variation and evolution of melt processes and how those processes might evolve on different timescales.

Modeled Discharge and Model Forcings

Modeled discharge is forced by both air temperature and solar radiation. First, hydrographs are plotted against mean air temperature (extrapolated from nearby weather station data) across the individual glacier surface (see Figure 16). Figure 17 presents hydrograph data compared to modeled solar radiation. Each hydrograph displays a sharp increase in melt volume as temperatures and solar radiation begin to rise, followed by a more gradual decrease, producing a tail at the end of the daily hydrograph. Comparing the results in Figure 16 and 17 shows this pattern more closely relates to the asymmetrical shape of the temperature data rather than the symmetrical solar radiation data. Additionally, peak timing of all three hydrographs correlate with peak air temperature and lag behind solar radiation by approximately 1 hour. Furthermore, all three modeled hydrographs exhibit low frequency variability that mimics variability observed in the temperature dataset, likely as a result of precipitation events. These precipitation events are especially evident in the Ulrichen pressure measurements. The lack of low frequency variability in the glacierized watersheds' pressure measurements

may be a function of the glacier's storage capacity and how precipitation flows on and through a glacier.

Although all three hydrographs are similar, differences do exist, particularly in the magnitude of melt amongst the three. The Gornergletscher, with the highest magnitude of melt, exhibits the lowest temperatures of the three; thus, we eliminate temperature as a driving factor behind this discrepancy. The difference is likely primarily a factor of glacier size and possibly also in part due to solar radiation; the Gornergletscher is considerably larger than the other two and experiences the highest solar radiation.

Modeled Discharge and Pressure Data

A strong correlation between air temperature, solar radiation, and modeled discharge can be observed in Figures 16 and 17. Figure 18 shows the same modeled discharge in two glaciated watersheds, the Rhonegletscher and Langgletscher, plotted with the corresponding pressure dataset. Here we see how closely the model mimics observations by comparing modeled results to measured data, though we note it is not a one-to-one comparison since we are comparing pressure to discharge data. However, the shape, duration, and timing of each peak should be relatable across these types of data. The timing of peak modeled discharge aligns with the timing of peak pressure in the measured dataset and captures the general shape of the pressure data. Thus, it is reasonable to assume that this model scenario described previously accurately captures the timing of peak melt. However, as mentioned previously, the model treats meltwater flowing across moraine material as surface flow. To determine if this approach best captures reality, we used Equation 7 and converted all surface flow across moraine

material to groundwater flow and analyzed the resulting hydrograph shape.

Alternative Moraine Flow

The watershed model treats all flow interacting with moraine material as surface flow due to the poor sorting and low permeability of the moraine material. However, to ensure that our model captures the ideal flow scenario, we explored alternate scenarios wherein the moraine is a more porous material and meltwater acts as groundwater percolating through the material. Doing so produces a significant delay in meltwater delivery traveling through moraine material, as seen in the hydrograph in Figure 19. The secondary peak observed in the daily hydrograph represents the volume of meltwater that must travel through the moraine material before reaching the glacier terminus and the proglacial stream system.

If the moraine material is treated as a poorly sorted medium with low permeability and high porosity, the meltwater is delayed significantly and the double peak smooths out, but with the peak melt significantly delayed relative to the pressure data. Moreover, the hydrograph loses its characteristic asymmetry. Thus, we conclude that by treating the moraine material as a rocky channel and the meltwater as surface flow, we create a model scenario that more realistically captures the timing of peak melt and shape of the hydrograph.

Hydrograph Separation

We performed a hydrograph separation on each of the three glaciated watersheds to compare melt magnitudes between ice and snow and determine if one dominates the

system, and therefore the timing of peak melt. Note that while snow and ice melt are separated, flow through moraine material is included in both. This method further allows a comparison between the delivery times of snow and ice melt to the down-valley stream system. A lag time observed in either snow or ice melt could potentially explain the tail observed in the daily hydrograph.

As seen in Figure 20, ice melt (blue) dominates the system while snow melt (red) contribution is much lower for these glaciers, at least during the peak melt season. Although there is no snow melt for the Rhonegletscher or Gornergletscher in the first ~150 hours, we still observe a tail in the hydrograph each day. Thus, we conclude that the tail and asymmetrical shape are due to the shape of the temperature forcing itself rather than a delay in snow melt. This suggests that snowpack has little effect on the timing of meltwater delivery to the terminus at the end of the melt season for these glaciers.

Additionally, the timing of ice melt corresponds to the timing of peak total melt (yellow) in all three glaciated watersheds, suggesting that ice melt controls the timing of peak melt in these three glaciated watersheds during the end of the melt season. Peak snow melt on the Rhonegletscher and Gornergletscher both occur with peak ice melt. However, peak snow melt on the Langgletscher exhibits a delay of a few hours. A number of factors could contribute to this delay. To further understand controls on snow melt delivery to the terminus, we next run the model with varying snowpack characteristics, including depth of snowpack and distribution of snowpack.

Snow Depth and Snowline Variations

As shown in Figure 21, snowpack drastically affects the timing of peak melt, likely driven by snowpack depth or distribution. To help address this, we ran the model under different snowpack scenarios, with maximum snowpack depths ranging from 3 m to 20 m. In each resulting hydrograph, no observable difference was noted. Thus, we conclude that percolation time to the base of the snowpack has negligible effect on the timing of meltwater delivery to the stream system. We note, though, that the model neglects several parameters related to the physical properties of snowpack that could affect percolation time.

In contrast, shifting the snowline on each glacier drastically changes the resultant hydrograph. Figure 21 shows three model runs for the three glaciated watersheds: one run with the average August 2015 snowline for each (yellow), a completely bare-ice glacier (snowline at the glacier head, blue), and a completely snow-covered glacier (snowline at the glacier terminus, red). We then compare the magnitude of melt and the timing of meltwater delivery between a normal late summer glacier surface, a bare ice glacier, and a completely snow-covered glacier.

As seen in the hydrographs, a bare ice glacier causes an increase in meltwater flux with little effect on shape of the hydrograph or the timing of meltwater delivery in all three glaciated watersheds. A snow-covered surface, however, yields smaller, broader peak volumes of meltwater delayed by approximately 1 hour on the Langgletscher and 4-5 hours on the Rhonegletscher and Gornergletscher. There is less of a delay on the Langgletscher due to its size; at only 6 km long, the travel time for meltwater is much lower than the other two glaciers. Covering a sufficiently large percentage of the

glacierized surface therefore changes the distribution of snowpack, drastically affecting the timing of meltwater delivery to the glacier terminus and downstream while simultaneously somewhat decreasing the asymmetry in the hydrograph.

To further investigate, we shifted the snowline in increments of 100 m to analyze the effect the snowline elevation has on the timing of peak melt. During August 2015, the snowline on the Rhonegletscher was at 3060 m. Approximately 39% of the glacierized surface was covered by snowpack. Snow melt delivery was delayed once the snowline is dropped to approximately 2900 m, or when approximately 62% of the glacierized surface was covered by snowpack. The results for the Gornergletscher are very similar to those for the Rhonegletscher. On the Gornergletscher, with an average August snowline of 3573 m, snowpack covered approximately 35% of the glacier surface. With this snowline, there was no time delay observed in snow melt delivery to the terminus. However, shifting the snowline elevation to 3200 m produced a significant offset in the timing of snow melt delivery to the glacier terminus; at this elevation, snowpack covered approximately 64% of the glacier surface. In contrast to these two glaciers, we observed an offset in the timing of snow melt delivery to the terminus of the Langgletscher for August snowline conditions without any artificial shifting of the snowline elevation. However, with an average August snowline of 3022 m, almost 50% of the glacier's surface was snow-covered, whereas the Rhonegletscher and Gornergletscher had a considerably lower snowpack percentage. Thus, we conclude that the snowpack distribution, rather than the snowpack depth, is the primary control on the timing of snowmelt delivery to the glacier terminus and that, on average, half the glacier's surface must be snow-covered before there is an observable offset in the proglacial hydrograph.

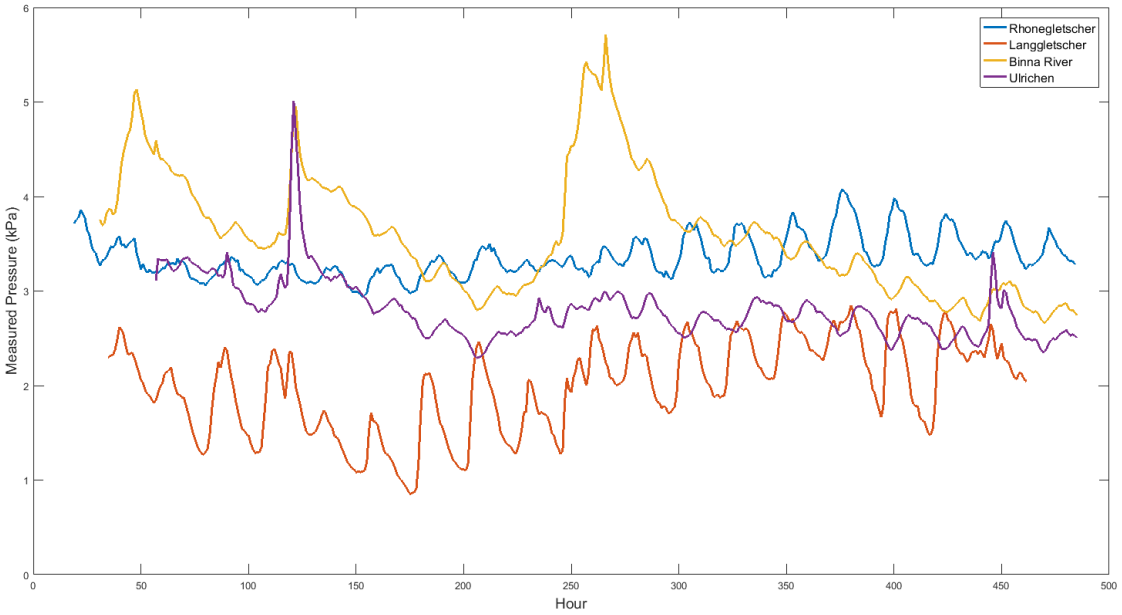

Figure 10. Pressure Transducer Data. Different colors represent data from the Rhonegletscher (blue), the Langgletscher (orange), and the two nonglacierized watersheds, the Binna River (yellow) and Ulrichen (purple).

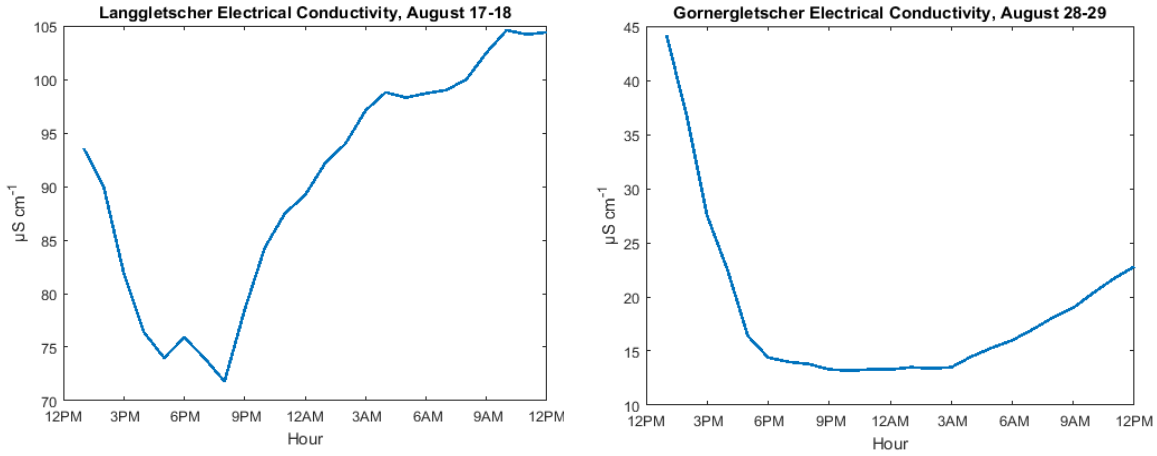

Figure 11. Electrical Conductivity Measurements from the Lang and Gornergletschers. Electrical conductivity begins to rise overnight when glacial contributions are at a minimum and continue to rise until the afternoon hours when glacial melt becomes the main contributor.

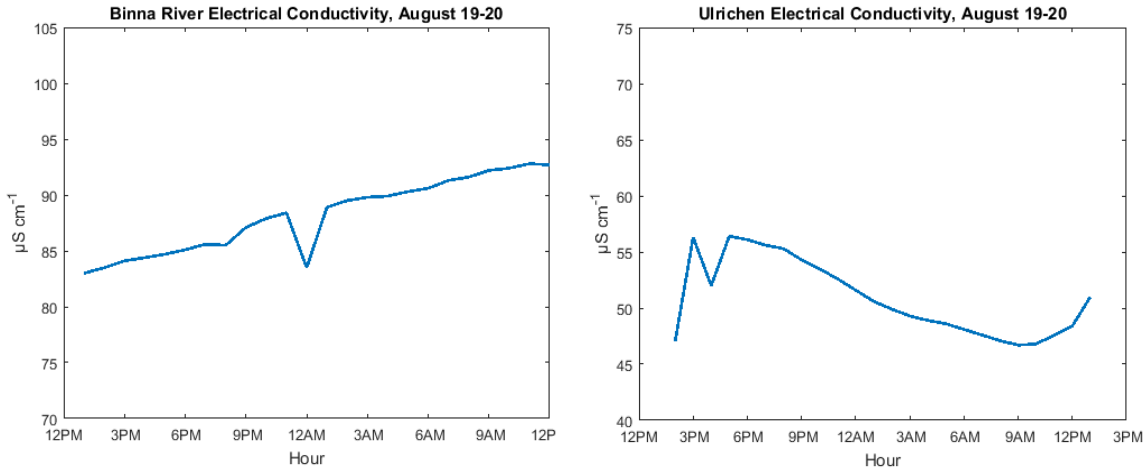

Figure 12. Electrical Conductivity Measurements from the Binna River and Ulrichen. Though magnitudes are similar to those measured in the glacierized catchments, there is no clear diurnal signal.

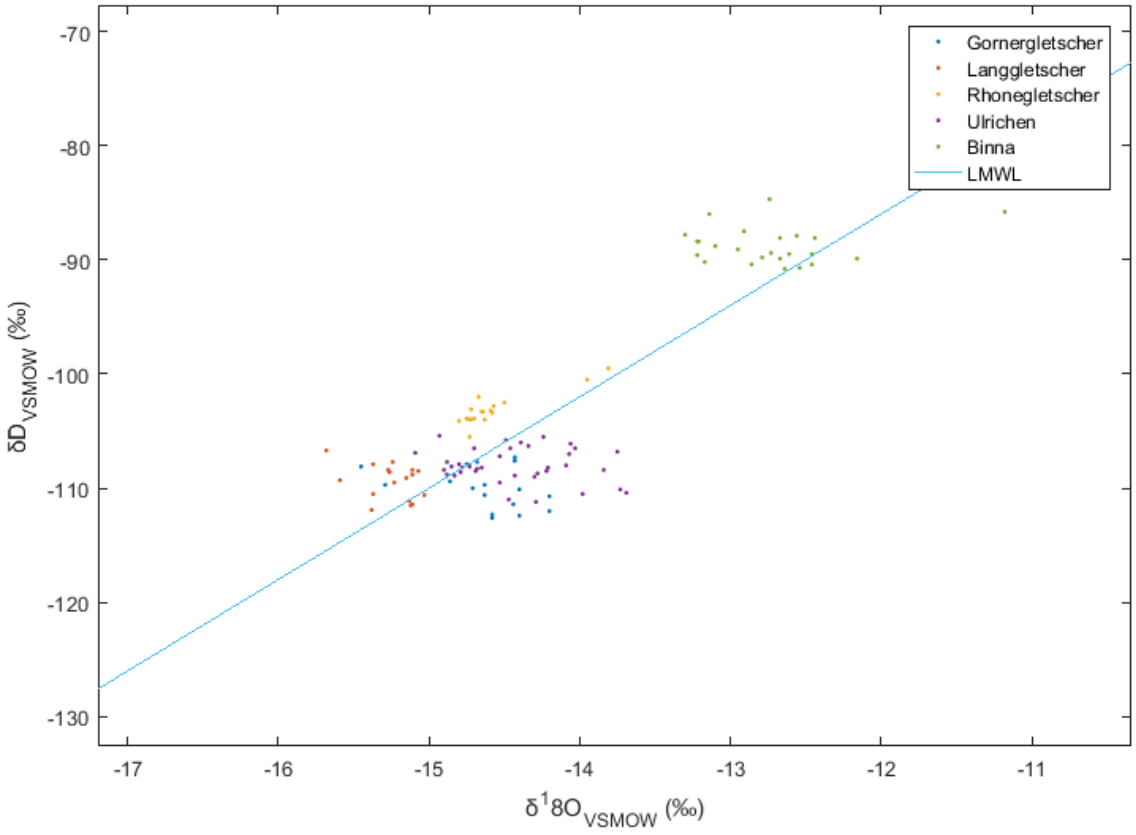

Figure 13. Stable Water Isotopes. All points represent samples collected in the Rhone Watershed during August 2015 during various hours of the day. Uncertainty is ± 0.20‰ for δ18O and ± 1.0‰ for δD. Included is the global meteoric water line for reference.

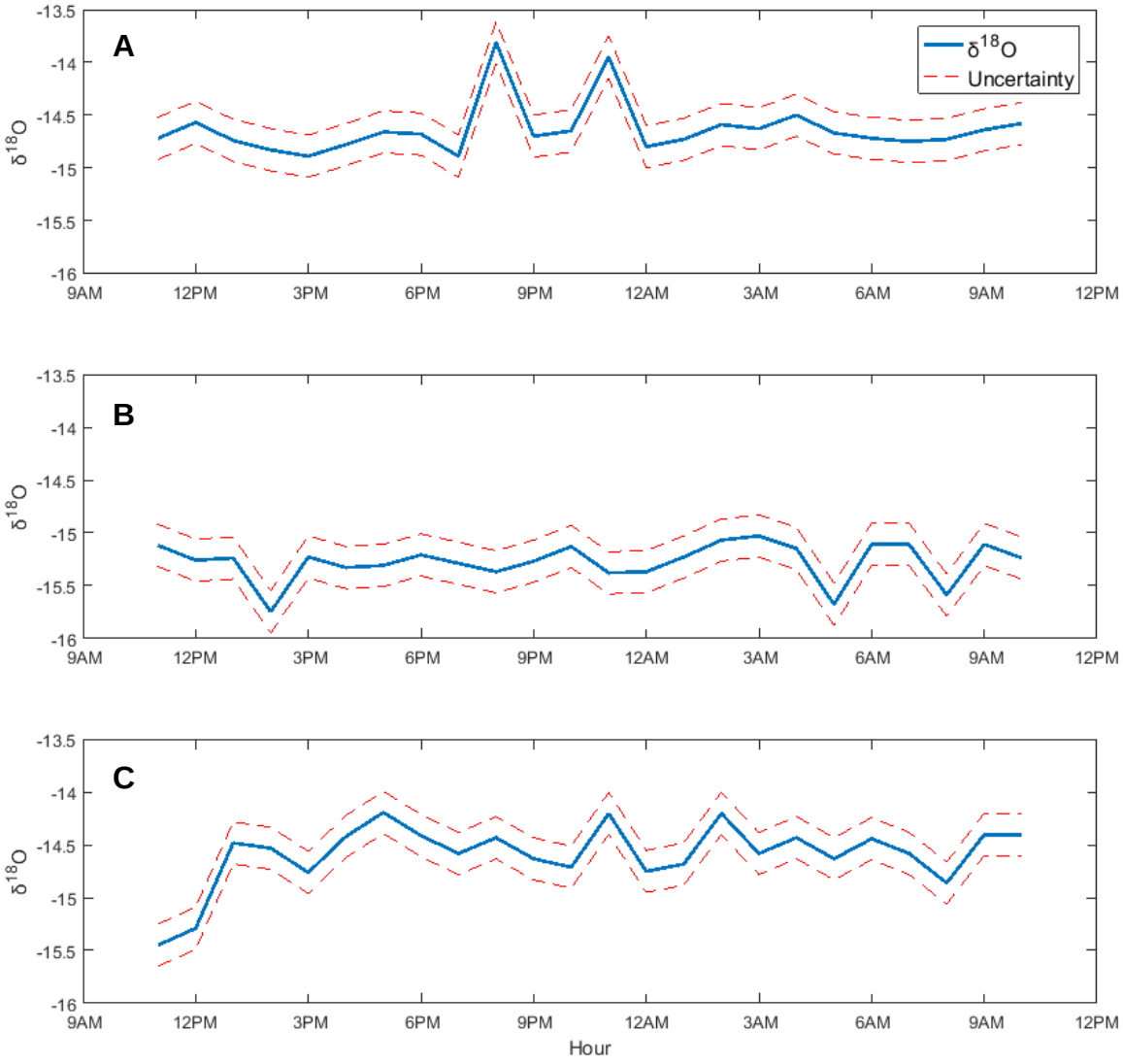

Figure 14. 24-hour Isotopic Measurements from the Glacierized Watersheds. All three (Rhonegletscher (A), the Langgletscher (B), and the Gornergletscher (C)) have depleted isotopic signatures consistent with those of glacier ice and meltwater (see Table 3). Most notably, we observe no diurnal signal in the 24-hour data, suggesting that all water sources are glacially derived at the sampling point.

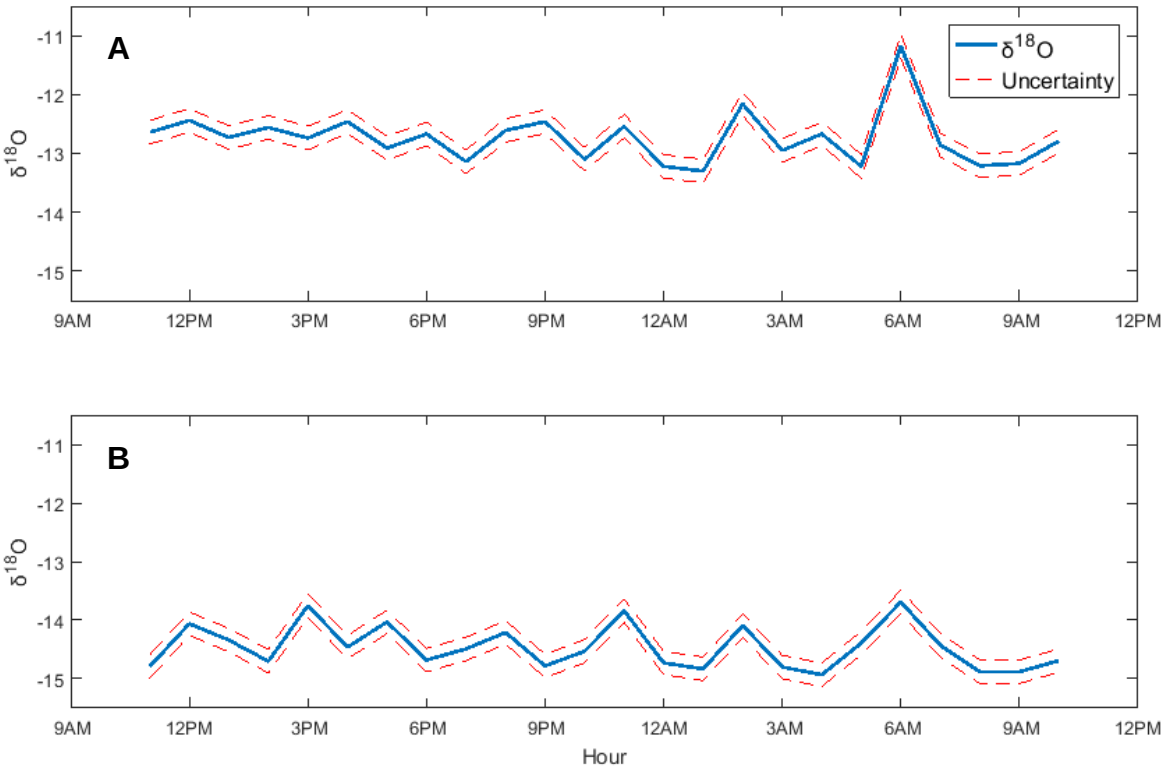

Figure 15. 24-hour Isotopic Measurements from the Nonglacierized Watersheds. Like the electrical conductivity measurements for these locations, there is no observable diurnal signal in the isotopic data (Binna River (A) and Ulrichen (B)).

Table 3. Isotopic signatures of ice samples, surface melt, and precipitation collected at various locations throughout the sampling period.

Sample	$\delta^{18}O$	Description
1	-13.36‰	Surface ice sample from the Rhonegletscher
2	-14.57‰	Surface ice sample from the Rhonegletscher
3	-15.31‰	Meltwater from the surface of the Rhonegletscher
4	-14.55‰	Meltwater from the proglacial lake at the toe of the Rhonegletscher
5	-16.58‰	Surface ice sample from the Langgletscher
6	-15.66‰	Precipitation at the Langgletscher sampling point

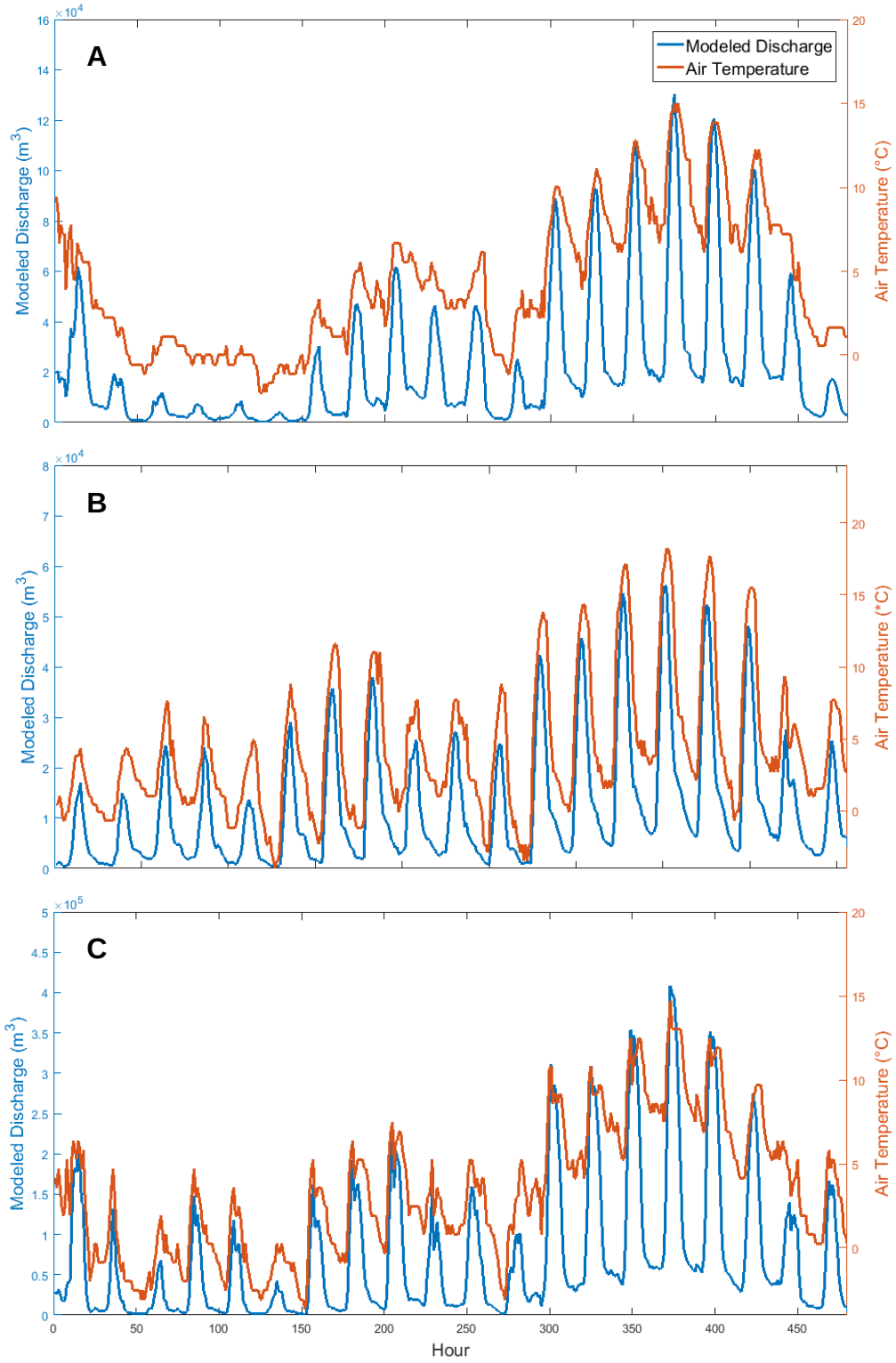

Figure 16. Modeled Hydrographs with Air Temperature. Model results are shown for the Rhonegletscher (A), Langgletscher (B), and Gornergletscher (C). All three align with peak temperature and appear to mimic the shape of the extrapolated temperature

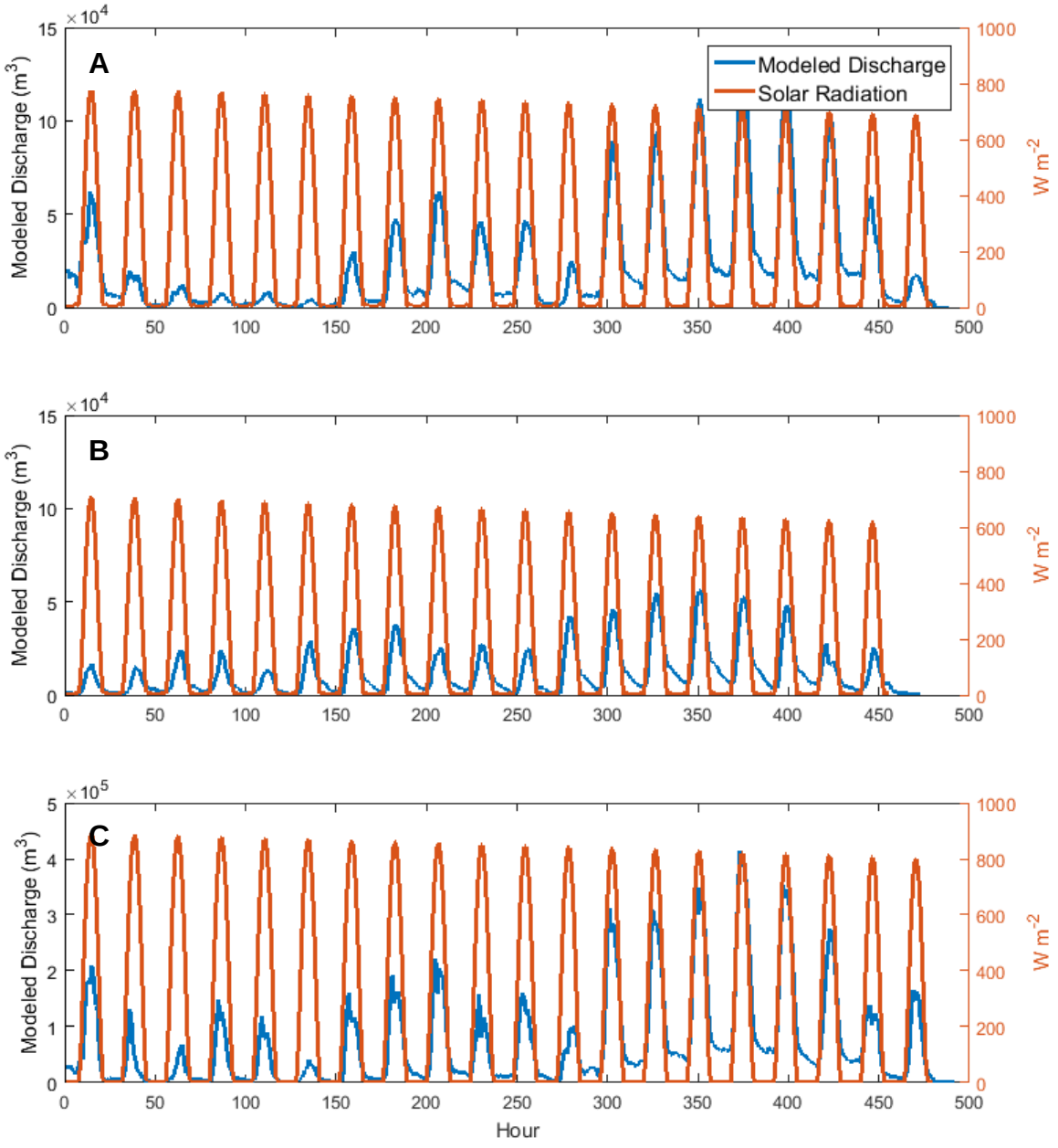

Figure 17. Modeled Hydrographs with Solar Radiation. Model results are shown for the Rhonegletscher (A), Langgletscher (B), and Gornergletscher (C) in blue and compared to modeled solar radiation (orange). The Gornergletscher has the highest solar radiation values and the highest magnitude discharge.

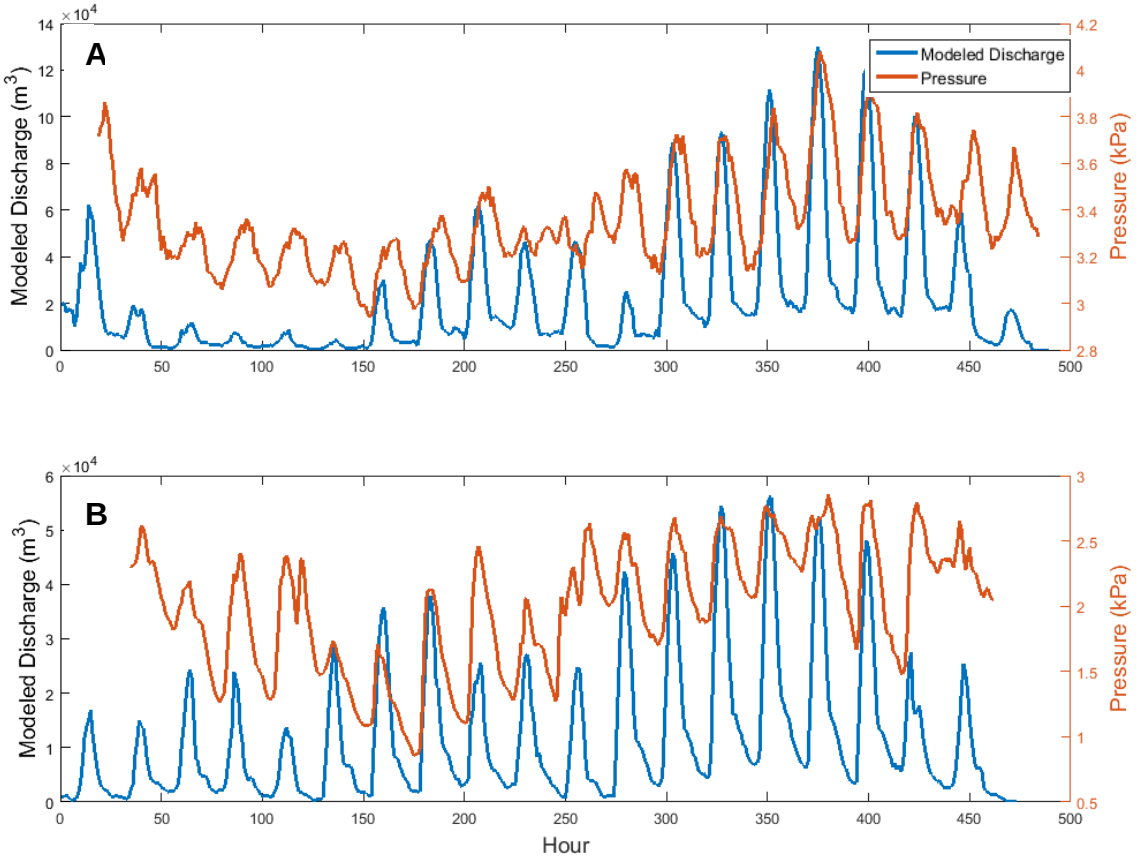

Figure 18. Modeled Hydrographs and Measured Pressure Data. Model results are shown for the Rhonegletscher (A) and Langgletscher (B) in blue, with pressure data in orange. Using the scenario in which moraine flow is treated as surface flow captures the timing of peak melt, as the peaks of the measured and modeled data align.

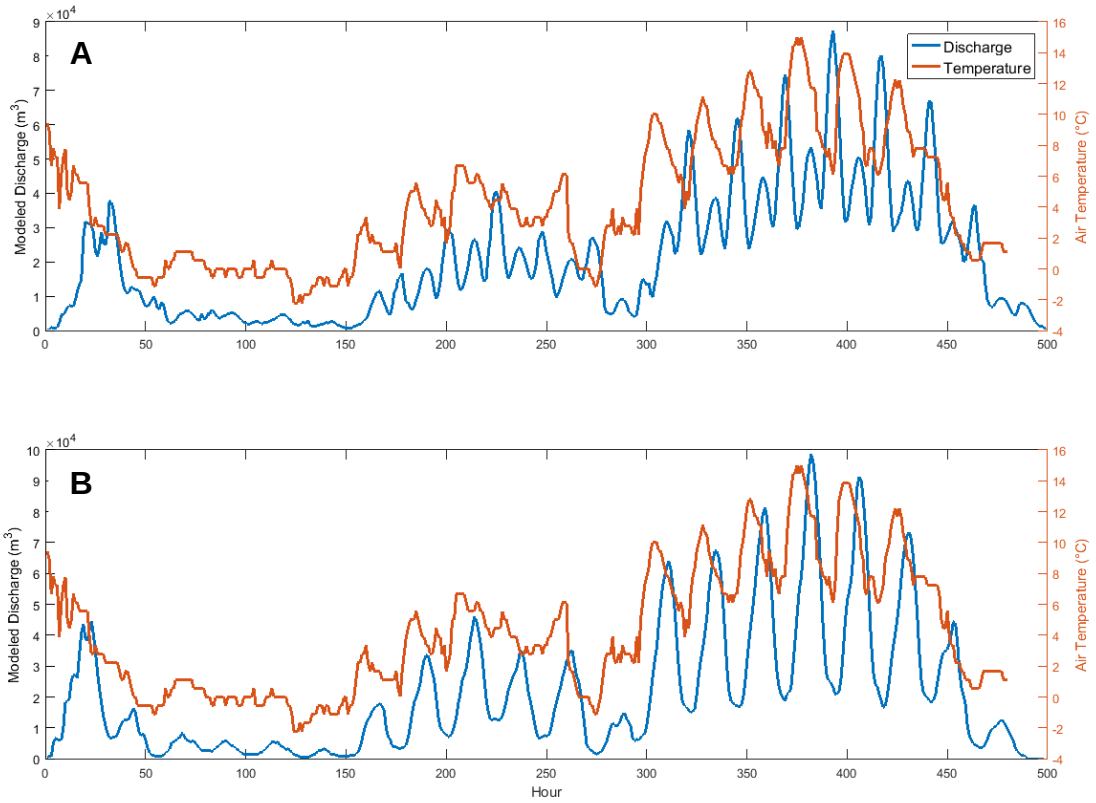

Figure 19. Alternative Moraine Flow Scenarios. In (A), the modeled hydrograph represents a scenario in which all meltwater flowing across moraine material percolates into the subsurface and flows as groundwater. We observe a peak during each daily cycle; the secondary peak represents all meltwater that flows through moraine material before reaching the terminus. In (B), we ran the same scenario but lowered the effective porosity of the moraine material. Doing so significantly offsets the timing of peak melt and smooths out the double peak.

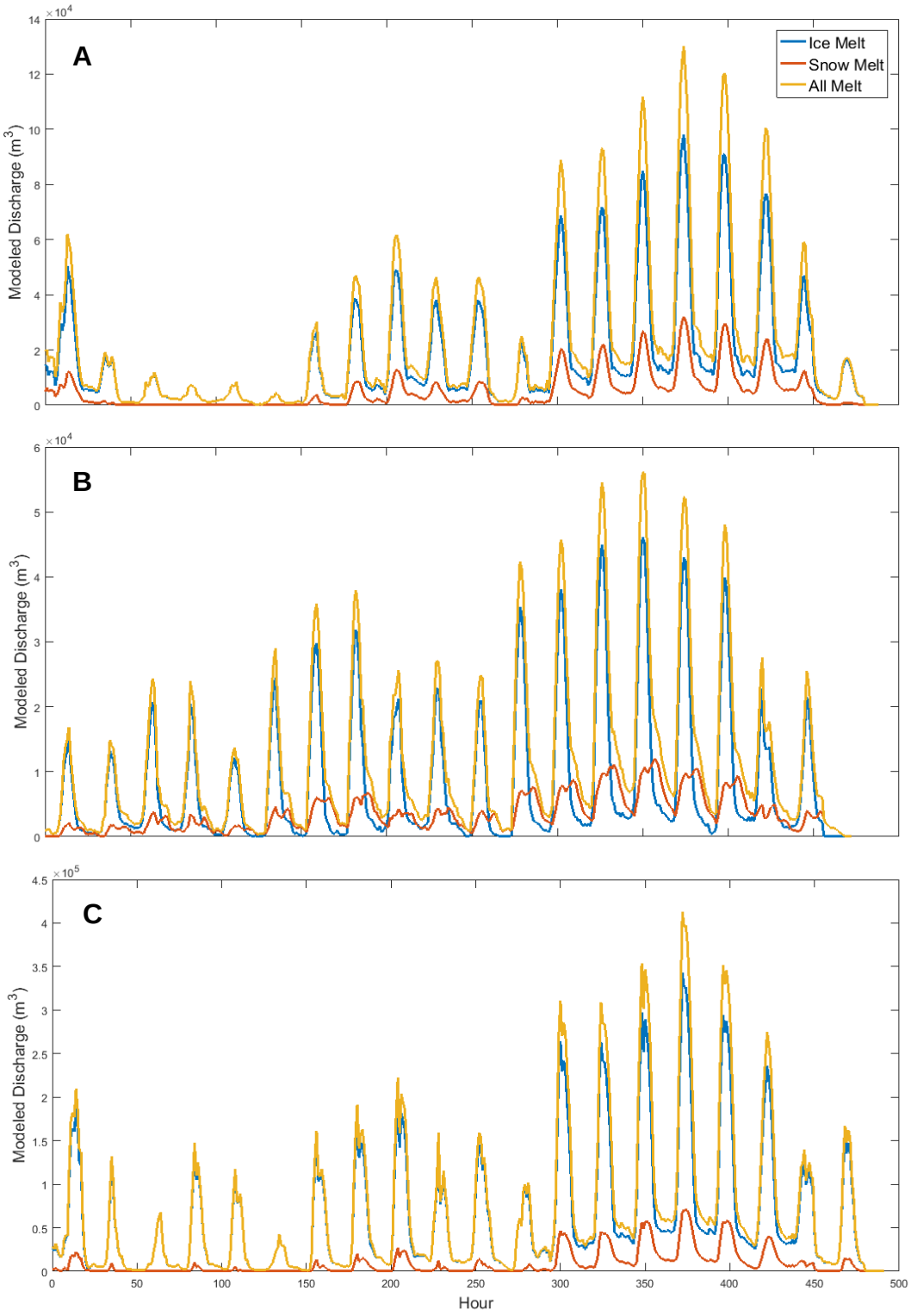

Figure 20. Hydrograph Separation. Snow and ice melt are separated for the Rhonegletscher (A), Langgletscher (B), and Gornergletscher (C). Both ice and snow melt hydrographs show a marked asymmetry.

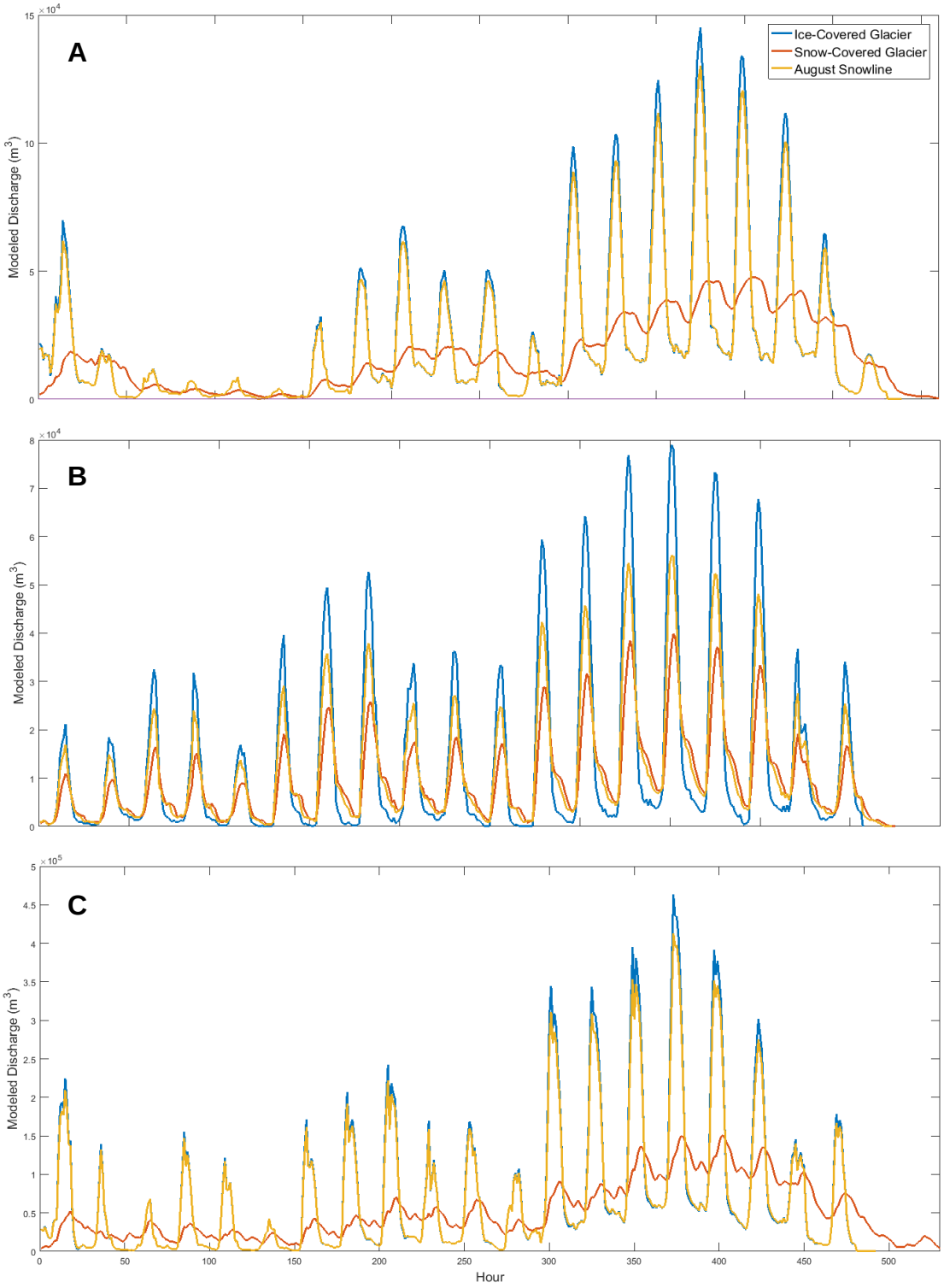

Figure 21. Varying Snowlines. The snowline elevation was artificially shifted for the Rhonegletscher (A), Langgletscher (B), and Gornergletscher (C). When the snowline is dropped to the terminus of the glacier, we see a delay in the timing of meltwater delivery on the Rhonegletscher and Gornergletscher.

DISCUSSION

Like all models, the melt and watershed models made simplifying assumptions and therefore inherits some limitations. Our major assumptions were: 1) within 2 km of the glacier terminus, all water contributing to the proglacial hydrograph was glacier runoff from snow and ice melt, and the groundwater contribution close to the terminus was negligible. This assumption is highly unlikely to be true; meltwater entering crevasses and moulins on the glacier surface will flow through subglacial conduits and tunnels, and run-off along the glacial periphery can take numerous potential paths (though moraines, subglacial systems, or deeper groundwater aquifers). Nevertheless, although these assumptions could change the magnitude of water flux in the river system, the modeled hydrographs capture peak timing and shape reasonably well, which is more pertinent to this study than actual magnitude.

The melt model also made simplifications that are relatively standard for temperature index models. For example, our temperature index model used a single melt factor, calculated as an average of six melt seasons (Gabbi et al., 2014) and corrected with radiation coefficients for snow and ice surfaces. However, in reality, melt factors are extremely sensitive and vary in time and space, even on small scales. Snow versus ice surfaces were determined by an average snowline calculation rather than a daily or weekly snowline calculation. The snowline was unlikely to change drastically over the short duration of the study, but it was also not stagnant. Additionally, the model assumed

clear sky conditions throughout the sampling period, and solar radiation was modeled rather than measured. For the solar radiation calculations, we used an average Earth-Sun distance for the month of August rather than the instantaneous distance each hour. Given these assumptions, the discharge magnitudes should be interpreted more as relative than absolute. However, the relative timing and rough magnitude of melt were reasonable and suffice for the purpose of this study.

In addition to the simplifications used in the temperature index model, our watershed model also contained simplifications. Most notably: 1) snow depth was linearly interpolated from the snowline to the maximum glacier elevation, with all cells at the snowline assigned a snow depth of 0.1 m and all cells at the head of the glacier assigned a snow depth of 5 m; 2) the model did not account for complex factors such as wind redistribution, avalanching, etc. that affect snow depth and distribution (although snow depth has little effect on the timing of meltwater delivery and hydrograph form, as demonstrated above, so these should have minimal effect on our results); 3) we assumed snow porosity and permeability were constant, with values selected to represent medium grained, old, dry snow; 4) the model did not account for stratigraphic horizons, ice lenses, or other low permeability snow layers within the snowpack that can cause a delay of meltwater percolation to the base of the snowpack, thereby potentially leading to an overestimation of runoff at the glacier terminus (Marsh and Woo, 1984; Fountain, 1996); and 5) the model did not account for a firn layer in the accumulation zone, though we expect the differences in timing and magnitude of model results would be negligible (Fountain, 1996). However, multiple sensitivity tests suggest that these assumptions, if accounted for, would not significantly alter results.

Furthermore, because all meltwater was treated as surface flow, we did not account for subglacial routing. As a first-order model, we aimed to identify drivers affecting the shape and timing of the proglacial hydrograph due to glacial surface melt and run-off, and we therefore neglect subglacial influences on the hydrograph. However, it is likely that late season subglacial flow is through well-developed tunnels rather than distributed conduits. Therefore, subglacial drainage should have a flow rate similar to that on the surface. However, this is less likely earlier in the season. Thus, because of the assumption of all surface flow, modeled results are likely an overestimation of surface melt volumes.

Additionally, the model did not include the residence time of meltwater in the recently formed proglacial lake at the terminus of the Rhonegletscher. From the proglacial lake, meltwater spills over a rock ledge and cascades down the rock face to form the Rhone River. Little research has been done to analyze the effect that the pooling of water in the proglacial lake and the timing of meltwater spilling over the ledge has on the hydrograph form. However, this should have a dampening and smoothing effect on the measured hydrograph.

Hydrograph Characteristics

Despite the assumptions above, the combination temperature index and watershed model accurately captures the timing of peak meltwater delivery to the glacier terminus and the stream system, as well as the approximate shape of the hydrograph. Additionally, the model shows that ice melt dominates the system and controls the timing of diurnal peak melt at the end of the melt season. Furthermore, the model suggests that during late

summer at the end of the melt season, there is no offset in the timing of snow melt delivery to the glacier terminus. Changing the snowpack depth had a negligible effect on the timing of snow melt delivery to the terminus. However, if we increased the area of the snowpack across the glacier surface by lowering the snowline elevation, results showed a time delay. We show that the glacier must, on average, be 50% snow-covered to yield any significant time delay. In addition, it has previously been reported that snowline elevation affects the shape of the hydrograph and that a snowline at the head of the glacier may eradicate the tail observed in the daily hydrograph (Willis et al., 2002). However, our modeled hydrographs still show a tail even with bare-ice glaciers.

The lack of delay of snow melt delivery to the glacier terminus observed in the late summer data suggests that, perhaps, at the end of the melt season, the tail observed in the proglacial hydrograph shape is no longer due to the delay in snow melt delivery to the terminus but rather becomes a function of air temperature. Air temperatures rise at a faster rate in the morning hours than the rate at which temperatures decreases later in the day, and the modeled discharge reflects this asymmetry. When the extrapolated weather station temperatures are replaced with a prescribed sinusoidal temperature, the tail disappears in the modeled hydrograph and the shape becomes symmetrical (see Figure 22).

Additionally, in Figure 22, we observe a decrease in peak melt volume throughout the modeled week. This is due to decreasing solar radiation over the course of the week. The modeled solar radiation is after the summer solstice, thus daily peak radiation decreases throughout the month of August, reducing the magnitude of melt slowly over time.

Channel Morphology

Rating curves for the Rhonegletscher and Langgletscher show the effect that braided channel morphology has on river stage (represented by pressure in Figures 23). The lowest river stages are associated with periods of low discharge (discharge < 10,000 $m^3\ hr^{-1}$) and represent base flow when surface melt is at a minimum; however, high river stages are not always associated with high discharge. This is due to channel morphology.

Pressure transducers were installed in main channels of braided systems. Data points with high river stages and lower discharge measurements (discharge < 30,000 $m^3\ hr^{-1}$) represent periods when the main channel system fills and reaches maximum river stage but significant volumes have yet to overflow to smaller sub-channels. This is especially apparent on the Rhonegletscher's rating curve, as there is more variability in the river stage and discharge relationship. Understanding how the rating curve is affected by river morphology is an important concept to consider when analyzing stream power, sediment load, and erosion rates. This also makes converting pressure transducer data to discharge data a significant challenge.

Future Work

First and foremost, the next step to creating a diurnal scale flow model is to account for the subglacial component and precipitation events. Including these will produce more refined results that may be beneficial for external use and lead to a calibrated model. However, doing so is beyond the scope of this project.

Additionally, more conclusive statements could be made by running the model on a seasonal timescale. By doing so, the model would include snowline elevation variations

(with lower snowlines earlier in the season) and would conclusively determine whether snowline elevation and the percentage of glacierized area under snowpack would affect the timing of snow melt delivery to the glacier terminus.

After identifying drivers in the system and developing a calibrated model, a high frequency runoff model could benefit several groups, including societies downstream and the local power sector. Hydropower production in the region is particularly susceptible to retreating glaciers and changes in meltwater flux downstream. Hydropower produces approximately 20% of the world's electricity and 56% of Switzerland's electricity (Finger et al., 2012, Gaudard et al., 2014). The Swiss hydropower market is worth approximately 1.8 billion CHF and comprises a major sector of the Swiss energy industry (Swiss Federal Office of Energy, 2014). Approximately one third of Swiss hydropower is produced in the Upper Rhone Watershed by eleven hydroelectric plants located along glacial tributaries to the Rhone River (Meile et al., 2011, Gaudard et al., 2014). One case study performed in the upper Saas Valley in the Upper Basin suggests that one hydropower reservoir will lose approximately 21% of its annual inflow by 2050 and decrease its productivity by 18% (Gaudard et al., 2014). Worldwide hydropower production is expected to decline by 6%; however, this number varies significantly by region. In the Alps, productivity may decline by 20-50% (Finger et al., 2012). There is much uncertainty associated with the future of hydropower in the Upper Rhone Watershed, and understanding melt patterns on different glaciers may help forecast water availability in the future.

Due to the importance of hydropower in the region, it will become increasingly important to understand controls on meltwater delivery downstream. By understanding

controls on high frequency variability, we can better understand variability on longer scales. Additionally, by understanding high frequency variability in the meltwater system, we can calculate stream power, which describes the efficiency in which a stream transports sediment and erodes the stream bed, on an hourly scale, which could have major implications on the hydropower sector. Over the course of nearly four decades, Hall et al. (2012) observed a decrease in stream power correlating with a decrease in snow cover and increase in air temperature. We expect stream power to increase in the Rhone Watershed as discharge increases. This could have major effects on hydropower reservoirs. Higher sediment fluxes reduce storage capacity and the lifespan of a hydropower reservoir. It has already been proposed that silt control dams be constructed to extend the life of hydropower reservoirs; however, understanding the controls on hourly meltwater flux and stream power could help determine future sediment flux estimates (Sabir et al., 2013).

Additionally, understanding controls on diurnal cycles and stream power will assist with future watershed management. In the Upper Rhone Valley, hundreds of thousands of people rely on meltwater for drinking water, agriculture, and irrigation. To manage this valuable resource, dams and channelization regulate flow on the Rhone River. Understanding these physical processes that control diurnal fluctuations will become increasingly important to ensure the success of these artificial structures as discharge increases. The societal importance of a physical model justifies the further study of high frequency variability in glacier dominated watersheds and highlights the importance of understanding drivers in the system that affect such variability.

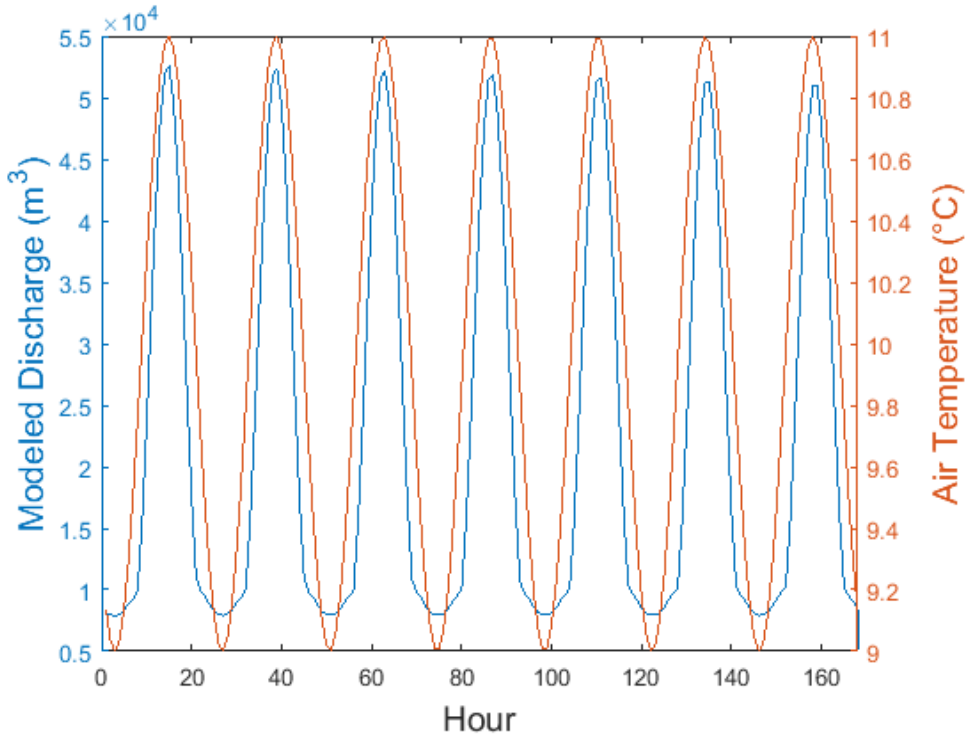

Figure 22. Modeled Discharge with a Sinusoidal Temperature Dataset. This particular graph shows results from the Rhonegletscher. A symmetrical temperature dataset yields a symmetrical hydrograph shape, suggesting that the tail observed in the proglacial hydrograph is largely temperature driven at the end of the melt season.

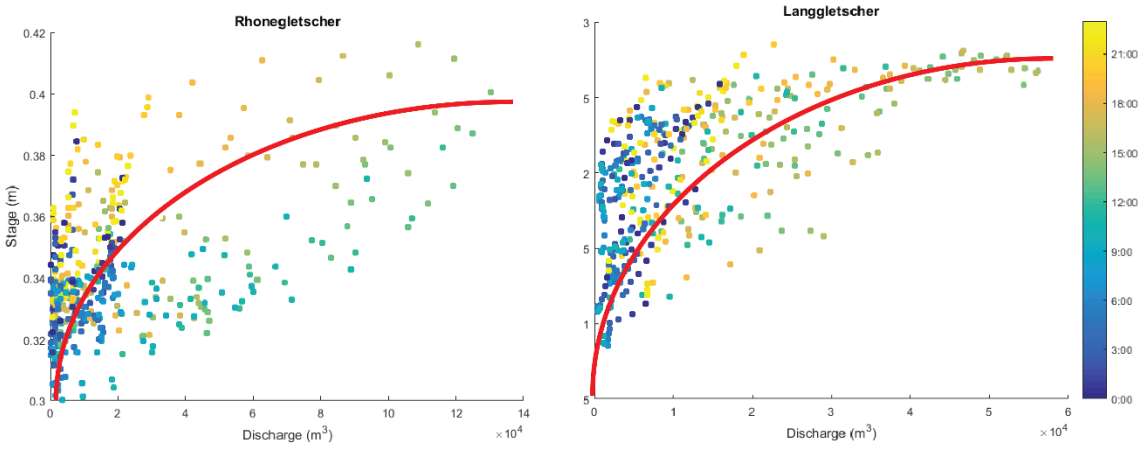

Figure 23. Rating Curves for the Proglacial Stream Systems. River stage is represented by measured pressure data in each watershed, and discharge is represented by model data.

CONCLUSION

Glaciers remain an important water resource in mountain regions throughout the world. While current models reproduce fairly accurate seasonal discharge measurements, many fail to capture daily cycles characteristic of proglacial hydrographs. It is important to understand high frequency variability and controls on meltwater delivery to the terminus, as high frequency variability could have substantial hydrological, ecological, and societal impacts.

High resolution pressure transducer data from two glaciated watersheds showed clear diurnal cycles, with a characteristic asymmetry of rapid increase in pressure followed by a slower decline in pressure. Diurnal cycles are also observed in the pressure data from two nonglacierized watersheds, though of a much smaller amplitude and much broader shape, with peak pressure occurring later in the day. These cycles in the glacierized watersheds are characteristic of glacier derived streams; we attribute the diurnal signal found in the nonglacierized watersheds to evapotranspiration. Source waters were determined in this study through isotopic analysis and electrical conductivity measurements to ensure that the majority of stream water measured was glacially derived and justified the use of pressure data as a comparison to modeled meltwater surface flow results. Hourly electrical conductivity measurements showed a clear diurnal cycle, with the highest electrical conductivity measurements appearing in the overnight to early morning hours. Isotopic signatures varied hour to hour with no clear diurnal cycle. If

source waters varied throughout the 24-hour period between a glacially derived source and another source such as groundwater, we would expect the isotopic signature to vary and show the most depleted values during maximum meltwater flow in the late afternoon and early evening hours. Because we observed a diurnal signal in the electrical conductivity and no signal in the isotopic data, it was determined that all stream water was glacially derived. Water passing through with the highest electrical conductivity was likely a subglacial, moraine, or other shallow groundwater contribution, originally sourced from glacial melt but having since undergone more interaction with rock.

A temperature index model calculated hourly melt across the glacierized surface, and the meltwater was routed to the sample location using a watershed model created in MATLAB. We compared modeled discharge measurements to physical data to validate the model. While acknowledging the model limitations and assumptions, the model did a reasonable job reconstructing the shape of the proglacial hydrograph and timing of peak melt.

In addition, the model was used to isolate factors that control said shape and timing. In this model, air temperature and snow distribution, rather than snow depth, had the largest effect on shape and timing. The asymmetrical proglacial hydrograph shape disappeared when the extrapolated air temperature dataset was replaced with a simulated sinusoidal temperature dataset; thus, we conclude that the asymmetrical tail is, in part, a function of air temperature. We conclude that snowpack distribution also has an effect on the timing of peak melt. During late summer at the end of the melt season, snowpack covered a small enough area across the glacier surface that the snowpack distribution had little effect on the hydrograph shape or timing. However, when the model's snowline

elevation was lowered and a larger percentage of the glacierized surface was covered in snow (at least 50% covered), the timing of peak melt was delayed by as much as 4-5 hours.

While the model successfully identified drivers and controls in the system, a carefully calibrated model, or validated physical model, is needed to help estimate future flow conditions. Doing so would require a subglacial component in the model. We would no longer assume all meltwater to flow along the surface before reaching the terminus; rather, some of the meltwater would be routed to moulins and crevasses and routed beneath the glacier. The hydropower sector in particular could benefit from a more accurate model. A model that quantifies high frequency variability could be used to estimate future flow conditions and stream power due to changes in magnitude and timing of the diurnal cycle. However, by identifying drivers and controls in the system, we create a framework to better understand the impact diurnal variations have on the various hydrologic, ecologic, and human systems that rely on glacial melt.

REFERENCES

Arnold, Neil, Richards, Keith, Willis, Ian, and Sharp, Martin, 1998, Initial Results from a Distributed, Physically Based Model of Glacier Hydrology: Hydrological Processes, v. 12, p. 191-219.

Beniston, M., Stoffel, M., and Hill, M., 2011, Impacts of Climatic Change on Water and Natural Hazards in the Alps: Can Current Water Governance Cope with Future Challenges? Examples from the European "ACQWA" Project: Environmental Science and Policy, v. 14, p. 734-743.

Bren, Leon J., 1997, Effects of Slope Vegetation Removal on the Diurnal Variations of a Small Mountain Stream: Water Resources Research, v. 33, no. 2, p. 321-331.

Brown, Giles H., 2002, Glacier Meltwater Hydrochemistry: Applied Geochemistry, v. 17, p. 855-883.

Cable, Jessica, Ogle, Kiona, and Williams, David, 2011, Contribution of Glacier Meltwater to Streamflow in the Wind River Range, Wyoming, Inferred via a Bayesian Mixing Model Applied to Isotopic Measurements: Hydrological Processes, v. 25, p. 2228-2236.

Ceppi, Paulo, Appenzaller, Christof, and Scherrer, Simon, 2009, Spatial Characteristics of Gridded Swiss Temperature Trends: Local and Large-Scale Influences [M.S. thesis]: Swiss Federal Institute of Technology Zurich.

Colbeck, S.C., 1978, The Physical Aspects of Water Flow Through Snow: Advances in Hydroscience, v. 11, p. 165-206.

Collins, David N., 2006, Variability of Runoff from Alpine Basins: Climate Variability and Change: Hydrological Impacts, p. 466-472.

Craig, H., 1961, Isotopic Variations in Meteoric Waters: Science, v. 133, p. 1833-1834.

Elliston, G.R., 1973, Water Movement Through the Gornergletscher: Symposium on the Hydrology of Glaciers, v. 95, p. 79-84.

Finger, David, Heinrich, Georg, Gobiet, Andreas, and Bauder, Andreas, 2012, Projections of Future Water Resources and Their Uncertainty in a Glacierized

Catchment in the Swiss Alps and the Subsequent Effects on Hydropower Production During the 21st Century: Water Resources Research, v. 48, p.

Flowers, Gwenn E., Clarke, and Garry K.C., 2002, A Multicomponent Coupled Model of Glacier Hydrology 1. Theory and Synthetic Examples: Journal of Geophysical Research, v. 107, p. ECV 9-1-ECV 9-17.

Fountain, Andrew G., 1996, Effect of Snow and Firn Hydrology on the Physical and Chemical Characteristics of Glacial Runoff: Hydrological Processes, v. 10, p. 509-521.

Fröhlich, C., 1993, Changes of Total Solar Irradiance: Interactions between Global Climate Systems: The Legacy of Hann. Washington, DC, American Geophysical Union, p. 123-129.

Gabbi, J., Carenzo, M., Pellicciotti, F., Bauder, A., and Funk, M., 2014, A Comparison of Empirical and Physically Based Glacier Surface Melt Models for Long-Term Simulations of Glacier Response: Journal of Glaciology, v. 60, p. 1140-1154.

Gaudard, Ludovic, Romerio, Franco, Dalla Valle, Francesco, Gorret, Roberta, Maran, Stefano, Ravazzani, Giovanni, Stoffel, Markus, and Volonterio, Michela, 2014, Climate Change Impacts on Hydropower in the Swiss and Italian Alps: Science of the Total Environment, v. 493, p. 1211-1221.

Glaciological Reports (1881-2015), 2015, The Swiss Glaciers: Yearbooks of the Cryospheric Commission of the Swiss Academy of Sciences (SCNAT) Published since 1964 by the Laboratory of Hydraulics, Hydrology, and Glaciology (VAW) of ETH Zürich, n. 1-132 (available at http://glaciology.ethz.ch/swiss-glaciers/).

GLIMS: Global Land Ice Measurements from Space, 2015, The Randolph Glacier Inventory 5.0: https://www.glims.org/RGI/rgi50_dl.html.

Gribovszki, Zoltán, Szilágyi, József, and Kalicz, Péter, 2010, Diurnal Fluctuations in Shallow Groundwater Levels and Streamflow Rates and Their Interpretation- A Review: Journal of Hydrology, v. 385, p. 371-383.

Hall, Dorothy K., Foster, James L., NiGirolamo, Nicolo E., and Riggs, George A., 2012, Snow Cover, Snowmelt Timing and Stream Power in the Wind River Range, Wyoming: Geomorphology, v. 137, p. 87-93.

Helfricht, K., Kuhn, M., Keuschnig, M., and Heilig, A., 2014, Lidar Snow Cover Studies on Glaciers in the Ötztal Alps (Austria): Comparison with Snow Depths Calculated from GPR Measurements: The Cryosphere, v. 8, p. 41-57.

Hock, Regine, 1998, Modelling of Glacier Melt and Discharge: Zürcher Geogr. Schr, 70.

Hock, Regine, 1999, A Distributed Temperature-Index Ice- and Snowmelt Model Including Potential Direct Solar Radiation: Journal of Glaciology, v. 45, n. 149, p. 101-111.

Hock, Regine, Jansson, Peter, and Braun, Ludwig N., 2005, Modelling the Response of Mountain Glacier Discharge to Climate Warming, in Huber, U.M., Bugmann, H.K.M., and Reasoner, M.A., eds., Global Change and Mountain Regions (A State of Knowledge Overview), Springer, Dordrecht, p. 243-252.

Howell, Wallace E., 1953, Some Measurements of Ablation, Melting, and Solar Absorption on a Glacier in Peru: Eos, Transactions American Geophysical Union, v. 34, n. 6, p. 883-888.

Huss, M., Bauder, A., Funk, M., and Hock, R., 2008, Determination of the Seasonal Mass Balance of Four Alpine Glaciers Since 1865: Journal of Geophysical Research, c. 113.

Iqbal, Muhammad, 1983, An Introduction to Solar Radiation: New York, Academic Press, Inc.

Keeler, D., Rupper, S., Bickmore, B., and Radebaugh, J., 2015, Development and Validation of a Physically Based ELA Model and Its Application to the Younger Dryas Event in the Graubünden Alps, Switzerland [M.S. thesis]: Brigham Young University.

Klok, E.J., Jasper, K., Roelofsma, Gurtz, J., and Badoux, A., 2001, Distributed Hydrological Modelling of a Heavily Glaciated Alpine River Basin: Hydrological Sciences Journal, v. 46, p. 553-570.

Kuhm M., Haslhofer, J., Nickus, U., and Schellander, H., 1998, Seasonal Development of Ion Concentration in a High Alpine Snow Pack: Atmospheric Environment, v. 32, p. 4041-4051.

La Frenniere, Jeff, Mark, and Bryan G., 2014, A Review of Methods for Estimating the Contribution of Glacial Meltwater to Total Watershed Discharge: Progress in Physical Geography, v. 38(2), p. 173-200.

Machguth, H., Eisen, O., Paul, F., and Hoelzle, M., 2006, Strong Spatial Variability of Snow Accumulation Observed with Helicopter-borne GPR on Two Adjacent Alpine Glaciers: Geophysical Research Letters, v. 33.

Male, D.H., and Gray, D.M., 1981, Snow Cover Ablation and Runoff: Handbook of Snow, p. 360-436.

Mark, Bryan G., and Seltzer, Geoffrey O., 2003, Tropical Glacier Meltwater Contribution to Stream Discharge: A Case Study in the Cordillera Blanca, Peru: Journal of

Glaciology, v. 49, no. 165, p. 271-281.

Marsh, Philip, and Woo, Ming-Ko, 1984, Wetting Front Advance and Freezing of Meltwater Within a Snow Cover 1. Observations in the Canadian Arctic: Water Resources Research, v. 20, no. 12, p. 1853-1864.

Meier, M.F., and Tangborn, W.V., 1961, Distinctive Characteristics of Glacier Runoff: US Geological Survey Professional Papers, v. 424.

Meile, T., Boillat, J.L., and Schleiss, A.J., 2011, Hydropeaking Indicators for Characterization of the Upper-Rhone River in Switzerland: Aquatic Sciences, v. 73, p. 171-182.

Mercanton, P.L., 1916, Mensurations au Glacier du Rhône 1874-1915: Nouv. Mém. Soc. Helv. Sei. nat.

NASA LP DAAC, 2011, L5 ETM+ Collection 1 Level-1 Imagery. USGS Earth Resources Observation and Science (EROS) Center (accessed February 2016).

NASA/METI, 2011, ASTER Global Digital Elevation Model (GDEM): Sioux Falls, South Dakota, NASA EOSDIS Land Processes DAAC, USGS Earth Resources Observation and Science (EROS) Center (accessed February 2016).

Ofterdinger, Ulrich Stefan, 2001, Ground Water Flow Systems in the Rotondo Granite, Central Alps (Switzerland) [Ph.D dissertation]: Swiss Federal Institute of Technology (ETH) Zürich.

Pellicciotti, F., Bauder, A., and Parola, M., 2010, Effect of Glaciers on Streamflow Trends in the Swiss Alps: Water Resources Research, v. 46.

Portland State Aerospace Society, 2004, A Quick Derivation Relating Altitude to Air Pressure: http://archive.psas.pdx.edu/RocketScience/PressureAltitude_Derived.pdf

Richard, L. and Tonnel, A., 1985, Contribution a L'étude Bioclimatique de L'arc Alpin. Doc. Cartogr. Ecol, v. 28, p.33-64.

Roethlisberger, H., 1963, The Rhone Glacier Surveys: International Association of Scientific Hydrology, p. 119-121.

Schwanghart, W., and Scherler, D., 2014, TopoToolbox 2- MATLAB-Based Software for Topographic Analysis and Modeling in Earth Surface Sciences: Earth Surface dynamics, v. 2, p. 1-7. [DOI: 10.5194/esurf-2-1-2014]

Sabir, Mohammad Amjad, Shafiq-Ur-Rehman, Syed, Umar, Muhammad, Waseem, Amir, Farooq, Muhammad, and Khan, Abdur Rehman, 2013, The Impact of Suspended

Sediment Load on Reservoir Siltation and Energy Production: a Case Study of the Indus River and Its Tributaries: Pol. J. Environ. Stud., v. 22, no. 1, 219-225.

Singh, Pratap, Karitashya, Umesh K., Ramasastri, K.S., and Kumar, Naresh, 2005, Diurnal Variations in Discharge and Suspended Sediment Concentration, Including Runoff-Delaying Characteristics of the Gangotri Glacier in the Garhwal Himalayas: Hydrological Processes, v. 19, p. 1445-1457.

Stahle, K., and Moore, R.D., 2006, Influence of Watershed Glacier Coverage on Summer Streamflow in British Columbia, Canada: Water Resources Research, v. 42.

Stroeven, A., va de Wal, R., and Oerlemans, J., 1989, Historic Front Variations of the Rhone Glacier: Simulations with an Ice Flow Model: Glacier Fluctuations and Climatic Change, v. 6, p. 391-405.

Sugiyama, Shin, Bauder, Andreas, Zahno, Conradin, and Funk, Martin, 2007, Evolution of Rhonegletscher, Switzerland, Over the Past 125 years and in the Future: Application of an Improved Flowline Model: Annals of Glaciology, v. 46, p. 268-274.

Swiss Federal Office of Energy, 2014, Hydropower: http://www.bfe.admin.ch/themen/00490/00491/?lang=en

Wendler, G., Trabant, D., and Benson, C., 1972, Hydrology of a Partly-Glacier-Covered Arctic Watershed: Proc. Symp. On the Role of Snow and Ice in Hydrology. Intern. Assoc. Sci. Hydrol., v. 10.

Willis, Ian C., Arnold, Neil S., and Brock, Ben W., 2002, Effect of Snowpack Removal on Energy Balance, Melt, and Runoff in a Small Supraglacial Catchment: Hydrological Processes, v. 16, p. 2721-2749.